



Research papers

Enhancing an agro-ecosystem model (AHC) for coupled simulation of water–vapor–heat–salt transport in freezing and thawing soils

Yutao Liu ^{a,b}, Xu Xu ^{a,b,*}, Yihao Xun ^{a,b}, Chen Sun ^{a,c}, Guanhua Huang ^{a,b}

^a State Key Laboratory of Efficient Utilization of Agricultural Water Resources, Beijing, PR China

^b Center for Agricultural Water Research, China Agricultural University, Beijing 100083, PR China

^c Institute of Environment and Sustainable Development in Agriculture, Chinese Academy of Agricultural Sciences, Beijing 100081, PR China

ARTICLE INFO

This manuscript was handled by Y Huang, Editor-in-Chief, with the assistance of Hanbo Yang, Associate Editor

Keywords:

Water-heat-solute transport
Salinity
Vapor flow
Soil freeze-thaw process
Simultaneous simulation

ABSTRACT

Soil freeze-thaw has significant effects on the agro-hydrological processes throughout the entire agricultural year, and its reasonable description is crucial to the usability of the agro-ecosystem models for seasonal frozen regions. This article introduces the development and improvement of an agro-ecosystem model AHC (Agro-Hydrological & chemical and Crop systems simulator) for simulating water–vapor–heat–salt transport in freezing and thawing soils. The improved version (AHC-2.1R) is proposed to numerically simulate soil water–heat–solute transport, soil nitrogen–carbon turnover, and crop growth with frost conditions. The model improvements mainly include: (1) incorporating more rigorous soil water–vapor–heat transport equations with provisions for freezing and thawing soils; (2) reconstructing the numerical procedure to solve water–heat coupled equations simultaneously; (3) adopting two special treatments (i.e., the limitation of net water flux into a node and the available energy-based method for a phase change) to avoid the instability caused by phase change; (4) introducing a new snowpack module to calculate the snow dynamics. Then, the model was tested and evaluated by: (1) the experimental case of soil column freezing test, and (2) the sunflower field case over two entire agricultural years in seasonal frozen regions. Good agreements were obtained between the simulated and observed data, including the soil water contents, salt contents/salinity concentration, soil temperature, and crop growth indicators. The soil water–solute–temperature dynamics, crop growth, and yield formation process, as well as the complex interactive effects, were reasonably interpreted with the AHC-2.1R. In addition, the sensitivity test and scenario analysis were also carried out to test the model's stability, reasonability, and the necessity of model improvements. Overall, the above improvements effectively enhanced the AHC model's ability to simulate soil freeze–thaw process and extended its applicability to support farmland water–salt–nitrogen management and crop production for seasonal frozen regions.

1. Introduction

Agro-ecosystem (or agro-hydrological) models can be defined as a quantitative scheme for simulating and predicting hydrological, chemical, and biological processes in soil-crop systems, considering the influence of various human and environmental factors (Sinclair and Seligman, 2000; Singh et al., 2006; Xu et al., 2018). They have become essential tools for comprehensively analyzing complex agro-ecosystem processes, evaluating agricultural practices, managing crop-water systems, and identifying optimal management strategies for policy analysis (Dorigo et al., 2007; Holzworth et al., 2014; Ren et al., 2016). The soil

water environments (especially moisture, salinity, temperature, and nutrition) have large impacts on plant growth, and their quantitative characterization is thus quite important for achieving efficient management of irrigation and fertilization. From the most fundamental perspective of soil water balance, the existing models could range from functional (often described as “tipping bucket”) to mechanistic ones (i.e., based on the Richards equation) (Soldevilla-Martinez et al., 2014; Mao et al., 2020; Kimball et al., 2023). Solving partial differential equations (also the modified forms) allows the mechanistic model to flexibly simulate the dynamic processes and the continuous water-solute-heat fluxes (both upward and downward) under different

* Corresponding author at: State Key Laboratory of Efficient Utilization of Agricultural Water Resources, Beijing 100083, PR China.

E-mail addresses: yliu@cau.edu.cn (Y. Liu), xushengwu@cau.edu.cn (X. Xu), gotoxunyh@cau.edu.cn (Y. Xun), sunchen@caas.cn (C. Sun), ghuang@cau.edu.cn (G. Huang).

management and/or climatic regimes. These physical-based models especially can provide high simulation accuracy and wide environmental adaptability, such as having advantages in simulating shallow water table soils, heterogeneous soils, or frozen soils (Feddes et al., 1988; Pferdmenges et al., 2020).

Currently, many physical-based mechanistic agro-ecosystem models have been developed by various research institutions (Xu et al., 2018; Pferdmenges et al., 2020; Mao et al., 2020). The development of the model initially starts with water and crop simulation and has expanded to cover solute transport and transformation (e.g., salt, nitrogen, phosphorous, and pesticide), soil carbon and nitrogen turnover, thermal migration, gas emissions, etc., forming a composite simulation function (Pferdmenges et al., 2020; Heinen et al., 2024; Šimůnek et al., 2024). So far, some models with excellent functions have emerged and become the mainstream or popular models, typically such as HYDRUS, SWAP, WAVEs, RZWQM, Daisy, WAVE, CoupModel, and SHAW (Šimůnek et al., 2005; Šimůnek et al., 2024; van Dam et al., 1997; Kroes et al., 2017; Dawes, 1993; Ahuja et al., 2000; Hansen, 2002; Vanclooster et al., 1995; Wan et al., 2021; Flerchinger and Saxton, 1989; Flerchinger, 2024). In fact, every model has its assumptions, characteristics, limitations, and adaptabilities (Sinclair and Seligman, 2000; Pferdmenges et al., 2020; Xu et al., 2018). Continuous efforts are also made to model improvements, mainly related to: (1) the fundamental transport mechanism (e.g., macropore transport, mobile-immobile transition, crack development, lateral drainage, and surface mulching) (Pferdmenges et al., 2020; Heinen et al., 2024); and (2) enrichment of the model functions, for example, adding crop growth functions for HYDRUS and SHAW, or applying hybrid use of different models (e.g., the linkage of SHAW with RZWQM, WOFOST or AHC to correct simulation of overwinter conditions) (Li et al., 2012; Li et al., 2013; Liu et al., 2024).

Particularly, in recent years, we have found that an old issue, “soil freeze-thaw process and simulation”, which this study focuses on, has received more attention in the vadose zone and agro-ecosystem modeling (Li et al., 2012; Ireson et al., 2013; Kurylyk and Watanabe, 2013; Wu et al., 2019; Zheng et al., 2021; Xie et al., 2021). This is proper because most of the released numerical agro-ecosystem models tend not to conduct or simplify soil freeze-thaw simulations (Li et al., 2012; Šimůnek et al., 2016; Xun et al., 2022). To our knowledge, only several mechanistic agro-ecosystem models (e.g., SHAW-SC and CoupModel) provide mature programs to simulate soil freezing and thawing (Xun et al., 2022; Hansen, 2002). More other models tend to use relatively simple methods, such as (1) employing less complexity levels of water-heat equations, and (2) simply applying negative temperature to directly reduce the soil hydraulic conductivity without considering the ice phase or using a simple energy-supply method to estimate the conversion between liquid soil water and ice (based on a fixed freezing point (e.g., 0 °C)) (Luo et al., 2000; Kroes and van Dam, 2003; Li et al., 2010; Xu et al., 2018). Actually, it is very difficult to solve the water–ice–heat differential equations stably and efficiently because of the high degree of nonlinearity and water-heat-vapor-ice coupling, particularly under various complicated field conditions (e.g., time-variable atmospheric boundary, possible full saturation in frozen layers, and multi-layered soil profile) (Zheng et al., 2021). However, studies demonstrate that oversimplification of soil freeze and thaw may lead to significant errors in modeling results, making it impossible to predict agricultural ecosystem processes well in seasonal frozen regions (Hansson et al., 2004; Li et al., 2012; Liu et al., 2024). This limits the use of the models in practical field management and policy analysis on the scale of the entire agricultural year.

Therefore, it is essential to enhance the simulation ability of soil freeze-thaw process for numerical agro-ecosystem models, with the accuracy and stability both meeting the requirements of practical applications. The AHC model is a one-dimensional (1-D) numerical physical agro-ecosystem model (Xu et al., 2018, 2023), which can simulate the soil water flow, solute transport (salt and nitrogen), heat transport, soil carbon–nitrogen turnover, and crop growth and yield formation

under various ambient environments. It has been successfully applied by many users to simulate and solve the issues of water saving, salinity control, efficient nitrogen use, carbon use, crop response to changing environments, etc. (e.g., Huang et al., 2022; Li et al., 2023; Tang et al., 2024; He and Liu, 2024). However, the released version 2.0 (noted as AHC-2.0) still struggles to simulate the soil frost conditions due to oversimplification. Thus, the main objective of this study is to completely redesign the water-heat calculation principles of AHC and realize a fully coupled, simultaneous simulation of soil water–vapor–heat transport, solute transfer, and crop growth under both frozen and non-frozen conditions. Meanwhile, an appropriate numerical and coupling approach is proposed to make the updated AHC model (version 2.1R; hereafter referred to as AHC-2.1R) both physically realistic and computationally stable and efficient in soil freezing/thawing simulation. Then, the freeze–thaw simulation capability of the AHC-2.1R was first tested and evaluated using the experimental data from the laboratory soil column freezing test. After that, the model was further tested with sunflower field experiments over two agricultural years in the Hetao Irrigation District (Hetao) of the upper Yellow River basin. The two cases were used to demonstrate the simulation reliability and field applicability of the updated AHC-2.1R for seasonal frozen regions.

2. Model description and theoretical modification

2.1. AHC model and main principles

The AHC (Agro-Hydrological & chemical and Crop systems simulator) model is a vertically 1-D numerical physical-based model developed for the simulation of agro-hydrological and ecosystem processes (Xu et al., 2018, 2023). The mathematical part consists of seven main modules related to surface runoff, evaporation and transpiration, soil water, solute, heat, soil nitrogen and carbon, and plants. The model is mainly based on the numerical solution of a series of partial differential equations to simulate the transport processes. It also provides two global methods (i.e., LH-OAT method and modified-MGA method) for joint application in parameter sensitivity analysis and inverse estimation. The source code is written in FORTRAN.

In the previous version (AHC-2.0), the regular form of the 1-D Richards equation (Eq. A1) is applied to describe the soil water flow, and the 1-D heat transfer is described with a general form of convection–dispersion equation (CDE, Eq. A2). Hence, like many other agro-ecosystem models, AHC-2.0 neglects the effect of water vapor diffusion and ice phase on water-heat transport. The model adopts the advection–dispersion equation (ADE, Eq. A3) to simulate the solute transport and transformation processes in a variably saturated rigid porous medium involving a sequential first-order decay. The model provides a detailed simulation for the transformation processes of soil carbon and nitrogen, including mineralization-immobilization, solid adsorption, nitrification, denitrification, volatilization, nitrous oxide (N_2O) emission, root nitrogen uptake (positive and active) involved in the chain equations. The soil evaporation and crop transpiration are calculated using the Penman-Monteith equation or Hargreaves equation. Crop growth and yield formation are optionally simulated with the moderate (modified) EPIC crop growth module (called EPIC_CGM), and the detailed WOFOST module (called WOFOST_CGM). A more detailed theoretical description of AHC-2.0 can be found in Xu et al. (2018) and Xu et al. (2023). In addition, the friendly GUI has been developed for the pre- and post-processing of datasets using the Visual Basic.NET (VB.NET) programming language.

The AHC-2.0 has already become a very reliable, physically-based tool to simulate water flow, solute transport and transformation (salt and nitrogen), soil carbon and nitrogen turnover, heat transport, and crop growth and yield in agricultural fields, especially under non-frozen conditions. However, in AHC-2.0, the soil frost conditions are just simulated simply: (1) reducing the soil hydraulic conductivity when soil temperature is below 0 °C; and (2) using a variable active-node method

to define the active zone and simulating water-solute transport during only the soil thawing period (Xu et al., 2018). Therefore, in this study, the new version AHC-2.1R is proposed to improve the simulation abilities of the soil freeze-thaw process for seasonal frozen regions. The model upgrade work primarily involves improving the model's water and heat theories, reconstructing the numerical calculation methods, and renewing the coupling and iteration approach (water-heat-solute modules), which will be described in detail in the following sections. The main calculation flow chart of AHC-2.1R is provided in Fig. 1.

2.2. Principle improvements: water-vapor-heat-salt transport in freezing and thawing soils

2.2.1. Soil water flow and upgrade

In AHC-2.1R, a modified Richards equation (Eq. (1)) is introduced to describe the soil water flow, replacing the regular Richards equation (Eq. A1) with provisions for freezing and thawing soils is written as follows:

$$\frac{\partial \theta}{\partial t} + \frac{\rho_i}{\rho_l} \frac{\partial \alpha}{\partial t} = \frac{\partial}{\partial z} \left[K(h) \left(\frac{\partial h}{\partial z} + 1 \right) \right] - \frac{1}{\rho_l} \frac{\partial q_v}{\partial z} - S_w(h) \quad (1)$$

where θ is the volumetric soil water content ($\text{cm}^3 \text{cm}^{-3}$), t is time (d), ρ_i is the bulk density of ice (g cm^{-3}), and ρ_l is the density of liquid water (g cm^{-3}), α is the volumetric ice content ($\text{cm}^3 \text{cm}^{-3}$), h is the soil water pressure head (cm), z is the vertical coordinate (cm, positive upward), K (h) is the unsaturated soil hydraulic conductivity (cm d^{-1}), q_v is the vapor flux in the soil ($\text{g cm}^{-2} \text{d}^{-1}$) which is calculated by Eq. A4, and S_w is the sink term of soil water flow ($\text{cm}^3 \text{cm}^{-3} \text{d}^{-1}$).

Compared to the regular Richards equation (Eq. A1), Eq. (1) includes two new terms $\frac{\rho_i}{\rho_l} \frac{\partial \alpha}{\partial t}$ and $-\frac{1}{\rho_l} \frac{\partial q_v}{\partial z}$ which represent the change in volumetric ice content and the net vapor flux into a layer, respectively. The first term is essential when soil freezing and thawing (with liquid water and solid ice) is important, such as during the winter season in cold regions. The second term is necessary when vapor movement is an important part of total water flux, such as in relatively dry soil conditions (i.e., with low liquid water content). Therefore, the updated more rigorous soil water module based on Eq. (1) can be used to simulate the water flow under both frozen and non-frozen conditions.

Eq. (1) has a highly non-linear property, mainly due to dependencies of the water content and hydraulic conductivity on the pressure head (i.e., $\theta(h)$ and $K(h)$), and due to freezing-thawing effects that relate the ice content with the temperature (i.e., $\alpha(T)$) (see section 2.2.3). The solution

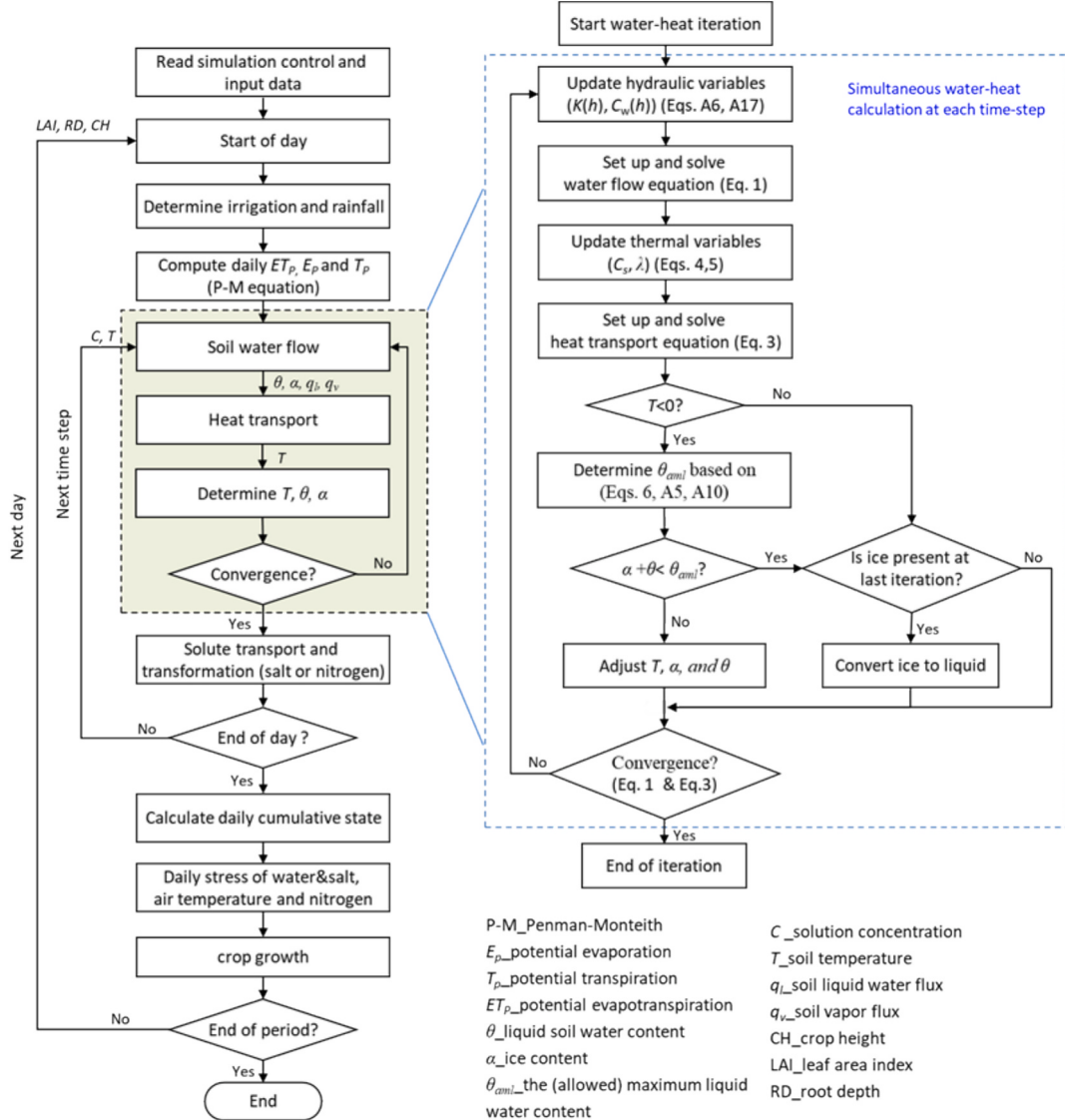


Fig. 1. The calculation procedure of the AHC model (The detailed water-heat coupling processes are addressed in the blue dashed box). (For interpretation of the references to colour in this figure legend, the reader is referred to the web version of this article.)

of Eq. (1) requires knowledge of both the soil hydraulic properties and the ice-temperature relationship. The soil hydraulic properties are still described by the van Genuchten-Mualem (VGM) model (Eqs. A5 and A6) (van Genuchten, 1980; Mualem, 1976). However, in AHC-2.1R, the hydraulic conductivity is reduced to account for the blocking effect of ice presence. Two approaches can be optionally used: (1) hydraulic conductivity is reduced linearly with ice content assuming zero conductivity at an available porosity of 0.13 (Bloomsburg and Wang, 1969); and (2) hydraulic conductivity is reduced by introducing an impedance factor (Ω , —), as follows:

$$K(h) = 10^{-\Omega Q} K(h) \quad (2)$$

where Q is the ratio of ice content to total (minus the residual) water content, which accounts for the fact that the blocking becomes more effective as the ice content part of the total water content increases (Hansson et al., 2004). The definition of initial conditions, boundary conditions, and source/sink terms is still similar to AHC-2.0, which can be found in detail in our previous paper (Xu et al., 2018).

2.2.2. Heat transport and upgrade

AHC-2.1R provides a more rigorous 1-D energy balance equation (Eq. (3)) for heat transport module, compared to the previous convection-dispersion equation (Eq. A2) used in AHC-2.0. The Eq. (3) can take into account both the existence of soil freezing and thawing in soil layers and the effect of the water vapor diffusion on heat transport, written as:

$$\frac{\partial C_s T}{\partial t} - L_f \rho_i \frac{\partial \alpha}{\partial t} + L_v \frac{\partial \rho_v}{\partial t} = \frac{\partial}{\partial z} \left(\lambda \frac{\partial T}{\partial z} \right) - \rho_l C_l \frac{\partial q_l T}{\partial z} - C_v \frac{\partial q_v T}{\partial z} - L_v \frac{\partial q_v}{\partial z} - S_h - \rho_l C_l S_w T_w \quad (3)$$

where C_s is the volumetric heat capacity of soil porous media ($J \text{ cm}^{-3} \text{ }^{\circ}\text{C}^{-1}$), C_l and C_v are the mass heat capacity (specific heat) ($J \text{ g}^{-1} \text{ }^{\circ}\text{C}^{-1}$) of liquid water and water vapor, respectively, L_f is the latent heat of ice fusion (335 J g^{-1}), L_v is the latent heat of evaporation (J g^{-1}), T and T_w are the soil temperature and the temperature ($^{\circ}\text{C}$) of inflow and outflow water, respectively, and λ is the coefficient of the apparent thermal conductivity of the soil ($\text{J cm}^{-1} \text{ }^{\circ}\text{C}^{-1} \text{ d}^{-1}$).

Compared to Eq. A2, there are four newly additional terms in Eq. (3). That is, the second and third terms on the left-hand side of Eq. (3) represent the changes in the latent heat of the frozen and vapor phases, respectively, the third and fourth terms on the right-hand side represent the transfer of sensible/latent heat by diffusion of water vapor, respectively. Note that the effects of ice are newly included in the calculation of heat capacity and thermal conductivity in AHC-2.1R, compared to AHC-2.0 (using Eqs. A7 and A8). Thus, the volumetric heat capacity and thermal conductivity, which now depends on the soil composition (mineral composition, organic matter contents, water, air, and ice), is calculated as a weighted mean of the heat capacities and conductivity of the individual component (Eqs. (4) and (5)), respectively.

$$C_s = f_{\text{sand}} C_{\text{sand}} + f_{\text{silt}} C_{\text{silt}} + f_{\text{clay}} C_{\text{clay}} + f_{\text{organic}} C_{\text{organic}} + \theta C_{\text{water}} + f_{\text{air}} C_{\text{air}} + \alpha C_{\text{ice}} \quad (4)$$

$$\lambda = \frac{k_w \theta \lambda_w + k_a \sigma_a \lambda_a + \sum_{i=1}^5 k_i \sigma_i \lambda_i}{k_w \theta + k_a \sigma_a + \sum_{i=1}^5 k_i \sigma_i} \quad (5)$$

where f and C are the volume fraction ($\text{cm}^3 \text{ cm}^{-3}$) and volumetric heat capacity ($\text{J cm}^{-3} \text{ }^{\circ}\text{C}^{-1}$) of each soil component, respectively, σ is the volumetric fraction of the component ($\text{cm}^3 \text{ cm}^{-3}$), k_{ic} is the ratio of the average temperature gradient in the kind of particular soil component to the average temperature gradient in a continuous medium (soil water or air). The subscript ic refers to a = air, w = unfrozen soil water, i = soil solid component ($i = 1 \dots j$ – soil minerals and ice), and j = number of individual types of soil solid components. The above approaches refer to De Vries (1963) and Tarnawski and Wagner (1992). The top and bottom

boundary conditions are both updated in AHC-2.1R. At the soil surface, the daily air temperature and the temperature of irrigation water are used to define the boundary conditions, and the daily fluctuations in air temperature can be represented by a sine function (Eq. A9). The bottom boundary condition can be specified as a zero heat flow or the third-type boundary condition in AHC-2.1R; and the latter is dependent on the prescribed temperature at the bottom.

2.2.3. Water-ice conversion and freezing-point depression equation

Unknowns in Eqs. (1), (A5) and (3) are soil water pressure head, water content, ice content, and temperature, and thus an additional equation is needed for a solution. This is provided by a modified form of the Clapeyron equation which relates liquid water pressure and osmotic pressure to equilibrium temperature in a soil system (without considering freezing-induced deformation), as follows (Cary and Mayland, 1972; Flerchinger, 2000; Fuchs et al., 1978):

$$\varphi = h + h_{so} = 10^5 \frac{L_f T}{g T_k} \quad (6)$$

where φ is the total potential of the soil water with ice present (cm), and h_{so} is the osmotic pressure of the soil solution (cm). This equation is referred to as the freezing point depression equation. It is used to define the relation between ice content and temperature in AHC-2.1R. The osmotic pressure h_{so} is estimated as a function of solute concentration and soil temperature by Eq. A10 (Hillel, 1998). Therefore, the (allowed) maximum liquid soil water content (θ_{am}) under freezing conditions could be determined by solving the Eqs. (A5), (6) and (A10). Soil water content (SWC) greater than θ_{am} is assumed to be ice in AHC-2.1R.

2.2.4. The snowpack

In AHC-2.1R, a relatively simple method is employed and adapted from SWAP v3.03 (Kroes and van Dam, 2003) to describe the snowpack dynamics, since it requires just the daily weather data. With the option to calculate snow accumulation and snowmelt for each day, the water balance of the snowpack on the soil surface will be calculated. This balance consists of several fluxes and a storage change in the snow layer. The incoming fluxes are the rain and snowfall. The outgoing fluxes are the snowmelt and sublimation.

The snow storage (S_{snow} , cm) is calculated as the storage of the previous day plus the precipitation minus the melt and sublimation (E_s , cm d^{-1}) amounts:

$$S_{\text{snow}}^{t+1} = S_{\text{snow}}^t + (P_r + P_s - q_{\text{melt}} - q_{\text{melt},r} - E_s) \Delta t \quad (7)$$

where P_r and P_s are the amount of rainfall on the snowpack and the snow depth (cm d^{-1}), respectively, q_{melt} is the amount of snowmelt (cm d^{-1}) due to air temperature rises above $0 \text{ }^{\circ}\text{C}$, $q_{\text{melt},r}$ is the amount of snowmelt (cm d^{-1}) due to heat released by splashing raindrops (cm d^{-1}), and E_s is the snow sublimation (cm d^{-1}). q_{melt} and $q_{\text{melt},r}$ are estimated using Eq. A11 and A12, respectively.

The melt fluxes leave the snowpack as runoff or infiltrate into the soil. The snow can also evaporate directly into the air, called sublimation. The sublimation rate is set equal to the potential evaporation rate. When a snowpack exists, the evaporation is first provided by the sublimation of the snowpack. If the amount of snow is insufficient, the surface evaporation then begins to come from the soil water. Moreover, in AHC-2.1R, when there is ponding water on the soil surface, we assume that if the average daily air temperature is less than $0.5 \text{ }^{\circ}\text{C}$ and surface soil temperature is below $0 \text{ }^{\circ}\text{C}$, all the ponding water will be frozen into ice. This treatment of the surface ice is similar to that of snowpack but with different parameters in order to simplify the calculation.

2.3. Numerical calculation procedures

2.3.1. Numerical Implementation

The water flow and energy equations (Eqs. (1) and (3)), subject to

appropriate initial and boundary conditions, are solved numerically using a fully implicit finite-difference scheme. Numerical discretization of Eqs. (1) and (3) can be expressed in finite difference forms as presented in Eq. A13 and A14, respectively. To make the program code more concise and efficient, AHC-2.1R employs an iterative Newton-Raphson technique to solve the above equations instead of using the modified Picard iteration in AHC-2.0. The solute ADE is still solved using the fully implicit or Crank-Nicholson, central finite-difference scheme, which is kept the same in AHC-2.0 (Xu et al., 2016); and the Picard iteration is applied and only needed for the conditions of non-linear adsorption for ADE.

Note that AHC applies a method of simultaneous solution of water flow and heat transport equations (Fig. 1), referring to the iteration approach of Flerchinger and Saxton (1989). It can effectively achieve numerical stability of water-heat coupling calculation. The variable to be solved for the water flow equation (Eq. (1)) is the pressure head h . The heat transport equation (Eq. (3)) has one unknown soil Temperature T . The solution for each time step involves alternating back and forth between a Newton-Raphson iteration for the water flow equation and one for the heat transport equation. An iteration is started to be conducted for the water flow equation, and two variables h and θ are calculated and updated (based on Eq. (1) and Eqs. A5-A6). This is followed by solving the heat transport equation in the current iteration, where T is calculated and updated; meantime, the ice content α is subsequently determined based on the T , h , and osmotic pressure, by solving Eqs. (A5), (6) and (A10). Upon completion of the iteration for the heat transport equation and ice freezing, the solution reverts back to an iteration for the water flow equation with the updated values (i.e., T , θ and α). In each time step, iteration continues until all subsequent iterations of both the water flow and heat transport equations for each soil compartment are within a prescribed tolerance (Flerchinger, 2000) (Fig. 1). This means that the water flow and heat transport equations are solved simultaneously. After iterations for the water flow and heat transport equations have reached convergence, solute transport is computed using the liquid fluxes from the water balance calculations.

2.3.2. Model stability treatment: freezing condition and saturation

(1) Freezing condition for heat transport

When the freezing point is reached, the apparent heat capacity (C_a , $J \text{ cm}^{-3} \text{ }^\circ\text{C}^{-1}$) will include the latent heat (stored in the ice) as an additional term in the soil heat capacity C_s and is calculated as:

$$C_a = C_s - L_f \rho_i \frac{d\alpha}{dT} = C_s + \rho_i L_f C_T \quad (8)$$

where C_T is the derivation of θ with respect to T , calculated by Eq. A15. The apparent heat capacity C_a increases by several orders (e.g., about two for silty clay and five for sand) of magnitude for soils when reaching the freezing point, compared to the value of only C_s . The significant changes in the C_a for temperatures above and below the freezing point can lead to significant numerical oscillations. This may result in oscillations in calculating temperatures between negative and positive values within a time step (Flerchinger, 2000; Hansson et al., 2004).

Thus, a method based on available energy for a phase change is adopted to avoid the above-mentioned oscillation or instability caused by a phase change (from liquid water to solid ice) in AHC-2.1R, as referred to Flerchinger (2000). For the iterative calculation of water and heat equations, the soil temperature is calculated using the heat CDE, and then the ice content of each frozen layer can be determined. When the temperature decreases from above to below freezing point, the new temperature should be adjusted as:

$$T_r = T_{fr} - \frac{E_{na}}{C_a} \quad (9)$$

where T_r is the revised soil temperature ($^\circ\text{C}$), E_{na} is the available energy for freezing (J cm^{-3}), and T_{fr} is the freezing point temperature ($^\circ\text{C}$). E_{na} is calculated as:

$$E_{na} = C_s (T_{fr} - T) \quad (10)$$

T_{fr} is lower than $0 \text{ }^\circ\text{C}$ for soils and can be derived from Eq. (6), as follows:

$$T_{fr} = T_k \cdot \frac{\varphi}{(10^5 L_f / g - \varphi)} \quad (11)$$

The above adjustment method is found to produce smooth calculations without undesired numerical oscillations, which also allows for larger time steps and reduces computation time for iterative calculations of soil water and heat equations.

(2) Limitation of net water flux when reaching full saturation

Under soil freezing conditions, it is possible that the net soil water flux into a node (or compartment) is greater than the available porosity in numerical calculation due to the presence of ice, especially when the soil moisture is high in the profile. This may cause an error in that the sum of the soil water content (θ) and the ice content (α) is greater than the saturated soil water content (θ_s). This would make the model unstable in soil freezing simulation when the medium reaches full saturation (Šimunek et al., 2016). To solve this problem, AHC limits net water flux into a node to be less than the available porosity (Φ_{av}) of that node.

The specific procedure starts from the bottom node and upwards to the top node, such as that for node i : (1) in case of the water flux (Q_{i-1}) through the top of the compartment moving downward into compartment i (positive upward), if the net water flux (i.e., $Q_i - Q_{i-1}$) beyond the Φ_{av} , the Q_{i-1} is adjusted into $Q'_{i-1} = Q_i - \Phi_{av}$ and the $K_{i-1/2}$ (i.e., mean hydraulic conductivity between the node i and the one above $i-1$) is set to zero at this iteration level. Meanwhile, if Q'_{i-1} becomes positive, it will be set to zero and Q_i will be updated into $Q'_i = \Phi_{av}$ (positive); (2) in case of the Q_{i-1} moving upward out of the compartment i (positive), if the net water flux beyond the Φ_{av} , the Q_i will be reduced into $Q'_i = Q_i - \Phi_{av}$ and $K_{i+1/2}$ is set to zero at this iteration level. In this way, AHC could effectively ensure the relationship of $\theta + \alpha \leq \theta_s$ for any node, and maintain the stability of numerical calculations for full saturation state.

3. Model testing and evaluation

In this paper, the AHC-2.1R was tested and evaluated using two datasets: (1) the experimental case of soil column freezing test, and (2) the sunflower field case over two entire agricultural years (agr-year, from October 1st to September 30th of the following year in the case region) in seasonal frozen regions. The experimental test served as a valuable benchmark for evaluating the numerical performance of the newly improved water-heat transport modules under controlled freezing conditions. The field case was used to further test the capability of the AHC-2.1R in simulating real complex soil freeze-thaw environments and to evaluate its calculation efficiency and field applicability.

3.1. Experimental case: soil column freezing test

3.1.1. Laboratory experiments

The data for the soil column freezing test were available from the previous studies (Mizoguchi, 1990; Hansson et al., 2004). Mizoguchi (1990) conducted an experiment using four identical cylinders filled with Kanagawa sandy loam, to investigate the coupled movement of water, heat, and solutes under soil freezing conditions. In this experiment, four soil columns were prepared by setting them to identical initial conditions (e.g., soil moisture and temperature), after which three columns were used for the freezing experiment.

The bottom and sides of the soil columns were encased with thermally insulated materials, while the top was placed in direct contact with an aluminum cooling tank to create a one-dimensional freezing condition. Before the experiment, the initial conditions in the soil columns were uniform, with an average temperature of 6.7 °C and a volumetric water content of approximately 0.34 cm³ cm⁻³ across the entire experimental domain. Then, the tops of the experimental columns were exposed to a circulating fluid of -6 °C with temperatures recorded by thermocouples. After 12, 24, and 50 h, the three experimental columns were removed from the freezing apparatus. Subsequently, soil samples from each column were sectioned into 1 cm thick slices, and the total water contents (TWCs, the sum of liquid water and ice contents) were measured. The schematic diagram of the experimental column setup and its discretization is shown in Fig. 2. The mean absolute error (MAE) was used in the laboratory freezing test to evaluate the model performance.

3.1.2. Model setup

According to the freezing experiments, a single soil profile with a 20 cm depth was used in the simulation. Then, the simulation domain was discretized into 20 compartments with a uniform thickness of 1 cm (Fig. 2). The simulation period was 150 h, covering the entire freezing experiment. The soil hydraulic parameters were determined and referred from Mizoguchi (1990) and Hansson et al. (2004) (Table 1). Texture for the Kanagawa sandy loam was estimated to be 70 % sand, 20 % silt, and 10 % clay, which was used to estimate the soil thermal properties with Eqs. (4) and (5).

For soil water flow, the upper and lower boundary conditions were set to zero flux boundary conditions. For heat transport, the lower

boundary was set to a zero heat flux because the bottom of the column was thermally insulated. Meanwhile, a variable heat flux boundary condition was applied at the top:

$$q_h = -\frac{h_c}{\Delta z} (T_1 - T_{fluid}) \quad (12)$$

where q_h is the heat flux (J cm⁻² d⁻¹) at the soil surface, h_c is the effective heat conductivity (J cm⁻¹ °C⁻¹ d⁻¹) at the top boundary affected by surface material, Δz is the 1/2 thickness of the surface compartment (cm), and T_1 and T_{fluid} are the temperatures (°C) of the soil surface and circulating fluid, respectively. According to a trial-and-error procedure similar to Hansson et al. (2004), the h_c used in our simulation was 300 J cm⁻¹ °C⁻¹ d⁻¹. A uniform soil salt content of 1 g NaCl kg⁻¹ soil was assumed in the simulation. The initial SWCs and temperatures were set based on the measurement of the fourth soil column.

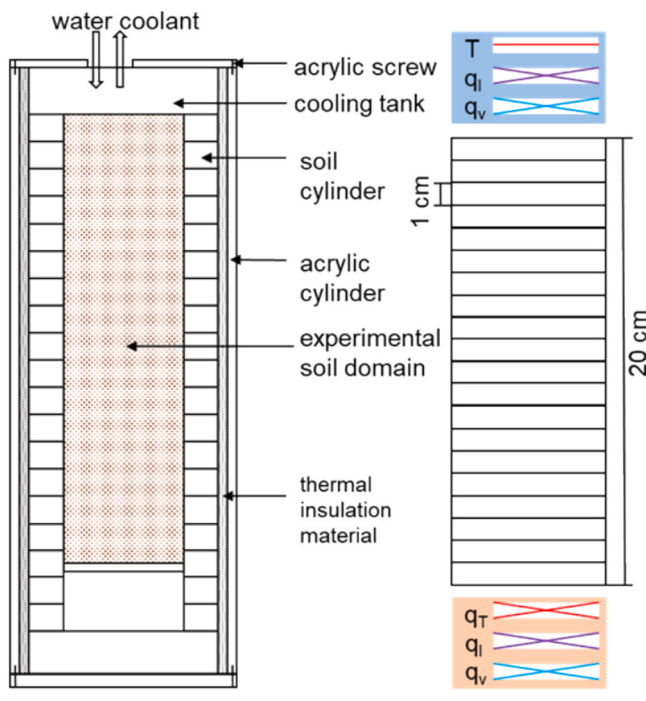
3.1.3. Simulation results and evaluation

(1) Calculation performance evaluation

The simulated TWCs and soil temperatures almost matched with the observed values, with similar trends of soil freezing to the experiment (Fig. 3). MAE was 0.0119, 0.0253, and 0.0199 cm³ cm⁻³ for TWCs at 12, 24, and 50 h, respectively. Simulation results confirmed that as freezing occurs, the soil water moved from the lower unfrozen layer to the upper frozen layer due to the soil water potential gradient. In addition, the upper soil temperature responded more quickly and decreased significantly faster than the lower one. The results of AHC-2.1R were also similar to those of SHAW (Fig. 3). However, there were still some differences between the two models, probably due to the different approaches in determining the soil porosity and considering the blocking effect of ice to reduce soil hydraulic conductivity. Moreover, the simulated soil temperatures in the deeper layer were slightly lower than the observed ones (Fig. 3b), and MAE for TWCs increased slightly with time. These were probably due to the poor insulation of the bottom and sides of the experimental columns, which led to the simulated freezing front going shallower than the possible one with perfect insulation conditions. Similar discrepancies between the observed and simulated TWCs were also found in the former research, such as by Hansson et al. (2004), Kelleners (2013), and Painter (2011) who studied the same laboratory freezing experiment with different numerical models. In addition, the MAE by AHC-2.1R was slightly larger than that by modified Hydrus-1D in Hansson et al. (2004). The reason may be caused by the different approaches used to determine the soil's thermal properties. The parameters of soil thermal conductivity in Hydrus-1D were estimated with an empirical equation (Eq. A16) (Campbell, 1985), while our research used the estimated soil texture and De Vries (1963) approach to determine the weighted average of conductivities for each component (Eq. (5)). Overall, the general agreement between our research's simulated and observed data indicates that the newly improved water-heat transport modules of AHC could reasonably simulate the dynamics of soil water and heat in the controlled laboratory experiment.

(2) Simulation analysis: the influence of various heat conductivity at top boundary

The heat conductivity at top soil boundary (h_c) is a calibrated value and can significantly influence the freeze-thaw process of soil. To verify the stability of our model, we did a series of simulations by changing the heat conductivity of material on the soil surface once at a time (similar to the sensitivity analysis) (Fig. 4a). It can be seen that as the soil surface heat conductivity became larger, the freezing depth went deeper into the soil domain, and the simulated frost depth almost reached the bottom of the soil profile after 50 h of freezing. However, it was found that if increasing the surface heat conductivity, the TWCs of top soils would



Boundary condition

- Specified upper boundary for constant temperature, zero liquid and vapor flux
- Specified bottom boundary condition for zero flux (heat, liquid water and vapor) boundary

T: temperature, q_T : heat flux, q_l : liquid water flux, q_v : water vapor flux

Fig. 2. Schematic diagram of the experimental setup and discretization of the soil column.

Table 1

Soil physical properties, soil hydraulic and transport parameters (calibrated values) in two simulation studies.

	Soil depth (cm)	Soil texture	Soil particle-size distribution (%)			Bulk density (g cm ⁻³)	Soil hydraulic parameters						Solute transport parameter L (cm)
			Sand (2.0–0.05 mm)	Silt (0.05–0.002 mm)	Clay (<0.002 mm)		θ_r (cm ³ cm ⁻³)	θ_s (cm ³ cm ⁻³)	α (cm ⁻¹)	n (–)	K_s (cm d ⁻¹)	λ (–)	
Lab	0–20	Sandy loam	70	20	10	1.1	0.05	0.535	0.011	1.48	27.65	0.5	1.25
Field	0–10	Sandy loam	58	35	7	1.6	0.05	0.42/ 0.3*	0.01	1.5	12/4*	0.5	30
	10–20	Sandy loam	58	35	7	1.6	0.05	0.42/ 0.35*	0.01	1.5	12/4*	0.5	20
	20–30	Sandy loam	58	35	7	1.6	0.05	0.42	0.01	1.5	12	0.5	20
	30–60	Loamy sand	79	19	2	1.48	0.05	0.43	0.01	1.5	16.8	0.5	20
	60–75	Silt	11	82	7	1.45	0.05	0.46	0.007	1.5	4.8	0.5	20
	75–180	Silt loam	44	53	3	1.55	0.05	0.46	0.007	1.5	16.8	0.5	20
	180–250	Silt loam	18	76	6	1.55	0.05	0.48	0.007	1.5	3.36	0.5	20
	250–300	Silt loam	40	54	6	1.55	0.05	0.48	0.012	1.5	19.2	0.5	20

Note: L refers to the longitudinal dispersivity for the salt solution. The superscript * means the parameter value was adjusted in the second agricultural year from 2020.10.6 to 2021.4.30 due to the compaction effect of large machines.

become smaller. This was probably caused by the differences in soil freezing rates. When the surface heat conductivity was small, it meant there was little cooling effect; and the rate of ice growth was relatively slow, thus more water could migrate from the lower layer to the upper frozen layer. But when the surface heat conductivity was large, there was more heat conductance transfer from the upper boundary to the soil surface, according to Eq. (12); and this meant there would be more negative heat transfer, and the cooling effect could be huge. More water would be frozen (in situ freezing) and the blocking effect of ice would dramatically reduce the moisture movement between soil layers, thus reducing the surface TWC with the increase of the surface thermal conductivity. To prove this hypothesis, we calculated the cumulative water flux of the surface node (Fig. 4b). After 5 h of freezing, the cumulative water flux decreased as the increasing of effective heat conductivity at the top boundary. Overall, the simulation and sensitivity analysis indicated that the AHC-2.1R could reasonably reflect the soil water-temperature dynamics and the responses to different values of surface heat conductivity.

3.2. Field case: entire agr-year simulation at a sunflower field in seasonal frozen regions

3.2.1. Site characteristics and observation data

In the field case, observation data were collected from the sunflower experimental fields over two agr-years (from October 2019 to September 2021) in the Yangchang canal command area (YCA), located in the Hetao Irrigation District (Hetao) of the upper Yellow River basin, northwest China ($40^{\circ}48'40''\text{N}$, $107^{\circ}05'15''\text{E}$). Hetao is characterized by a semi-arid to arid continental climate and is influenced by seasonal freeze-thaw cycles. The average pan evaporation (20 cm pan) is over ten times higher than the annual rainfall, with approximately three-quarters of the rainfall occurring between June and September (Xu et al., 2010). Due to the limited rainfall and dry climate in Hetao, crop growth is highly dependent on irrigation water mainly diverted from the Yellow River. The weather is cold and dry in winter, and the soil generally starts to freeze in mid-November and completely thaw in mid to late April, with frost days lasting over 150 days. Moreover, excessive canal irrigation and inadequate drainage result in shallow groundwater depth (GWD) in Hetao, typically ranging from 0.3 to 3.0 m (Mu et al., 2023).

In the field experiment, the sunflower was sown in early June and harvested in late September for both agr-years. Border irrigation was applied with an average salinity concentration of 0.5 g L^{-1} . The detailed crop cultivation, irrigation scheduling, and plastic mulching data are

listed in Table 2. Six soil horizons were observed for the soil profile, while the surface soil layer may be compacted by machine during land leveling in the second agr-year. The soil sampling was taken at an increment of 10 cm and 20 cm for the top layers (0–20 cm) and the below layers (20–100 cm), respectively. The SWCs and soil salt contents (g kg^{-1}) (SSCs) were measured with a soil auger every 7–15 days. Soil temperature and groundwater depth (GWD) were automatically monitored by a data logger. Leaf area index (LAI) and dry above-ground biomass (D-AGB) were measured at the same frequency as soil water, and the dry grain yield was weighted after harvest. The detailed measurement methods can be found in our previous study (Xun et al., 2022). Daily meteorological data for the two agr-years (from 2019 to 2021) was collected from the nearby Linhe Weather Station. The detailed daily weather data about relative humidity, air temperature, rainfall, and radiation are shown in Fig. 5 for both two agr-years.

3.2.2. Model setup

Soil water flow, solute transport, and temperature redistribution were computed for a soil profile with 300 cm depth and was divided into six horizons according to the soil texture distribution (Table 1). Then, the vertical one-dimensional soil domain was discretized into 300 soil compartments (nodes) with a uniform thickness of 1 cm. The simulation period was from October 1st to late September of the following years, covering the entire soil freeze-thaw period and the crop season of sunflowers (Table 2).

The observed SWCs, soil salinity concentration (C_{sw}), and temperature were used to define the initial conditions for 0–100 cm depth. Meanwhile, the initial conditions for the lower soils were inferred and estimated based on the observed GWD, total dissolved solids (TDS), and temperature of groundwater. For soil water flow, the upper boundary was determined by the actual soil evaporation and plant transpiration, as well as the irrigation and precipitation fluxes. At the bottom, the Dirichlet boundary condition was adopted by specifying the variable pressure head of the bottom node according to the monitored GWD. For heat transport, the top boundary condition was specified as the third type, which was defined based on the air temperature and incoming water (rainfall/irrigation). The lower boundary condition was determined by setting the bottom temperature equal to the temperature of groundwater. For solute transport, no solute is lost from the soil profile at the surface during evaporation, and the third type condition was applied during the infiltration process. The lower boundary condition was the first type of boundary condition with a given salinity concentration according to the measured TDS of the groundwater. The related

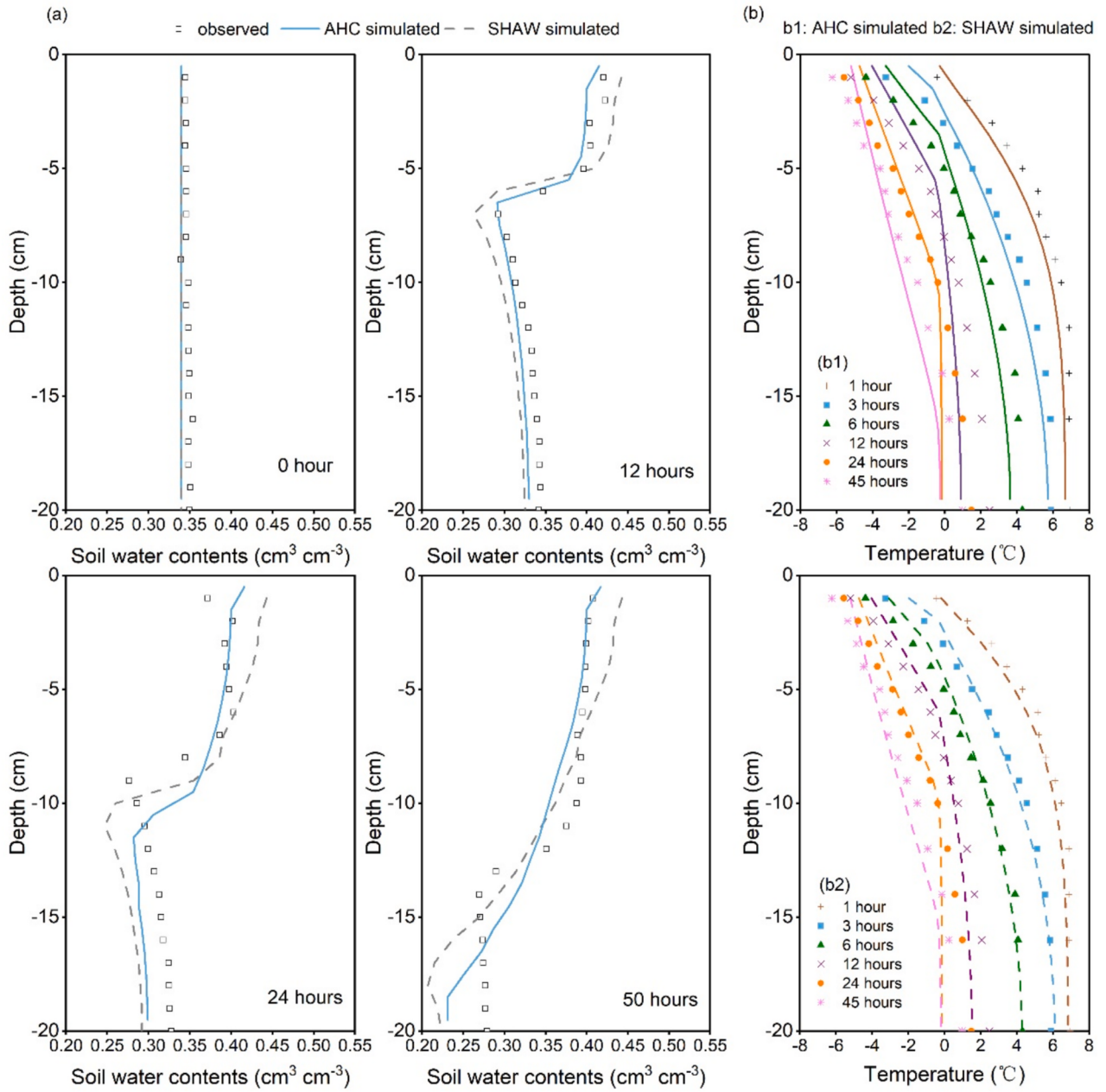


Fig. 3. Simulated versus observed soil water contents (a) and temperatures (b) of the experimental columns in different soil layers.

specific setting can be found in Xun et al. (2022) in detail.

The soil hydraulic parameters and parameters related to solute transport, heat transport, surface mulching, and crop growth were the main parameters for calibration. For soil water flow, the parameters (K_s , θ_r , θ_s , n , l , α) of the van Genuchten-Mualem equation were referred to Xun et al. (2022). To consider the compaction effect of the large machine during the land leveling at the beginning of the second agricultural year, the K_s (cm d⁻¹) and θ_s (cm³ cm⁻³) in 0–10 cm and 10–20 cm were slightly adjusted on October 6, 2020, and then restored to original values on April 30, 2021 (Table 1). This was carried out based on a trial-and-error approach to fit the observation data at field. That is, θ_s was adjusted from 0.42 to 0.3 and 0.35 in the first and second soil layers, respectively, and K_s was adjusted from 12 to 4 in these two layers. For solute transport, the longitudinal dispersivity (L) was set as 20–30 cm for the field scale. For heat transport parameters, a trial-and-error method was used to determine the h_c value. For surface mulching parameters, c_{mul} was determined during the field experiment, and f_{mm} was set

according to the mulch material (Allen et al., 1998). For crop growth, the related parameters were specified according to Xiong et al. (2019) and Xun et al. (2022). All the above-mentioned parameters may also be calibrated using a trial-and-error approach analogous to that adopted by Xu et al. (2013). The observed layered SWCs, C_{sw} , soil temperatures, and crop growth indicators (LAI and D-AGB) were used for model calibration (2019–2020) and validation (2020–2021). The mean relative error (MRE), root mean square error (RMSE), Nash and Sutcliffe model efficiency (NSE), and coefficient of determination (R^2) were used to evaluate the model performance for the field case. The definitions of the above goodness-of-fit indicators can be found in Xu et al. (2013).

3.2.3. Simulation results and evaluation

(1) Model calibration and validation

Referring to our previous research (Xun et al., 2022), the entire agr-

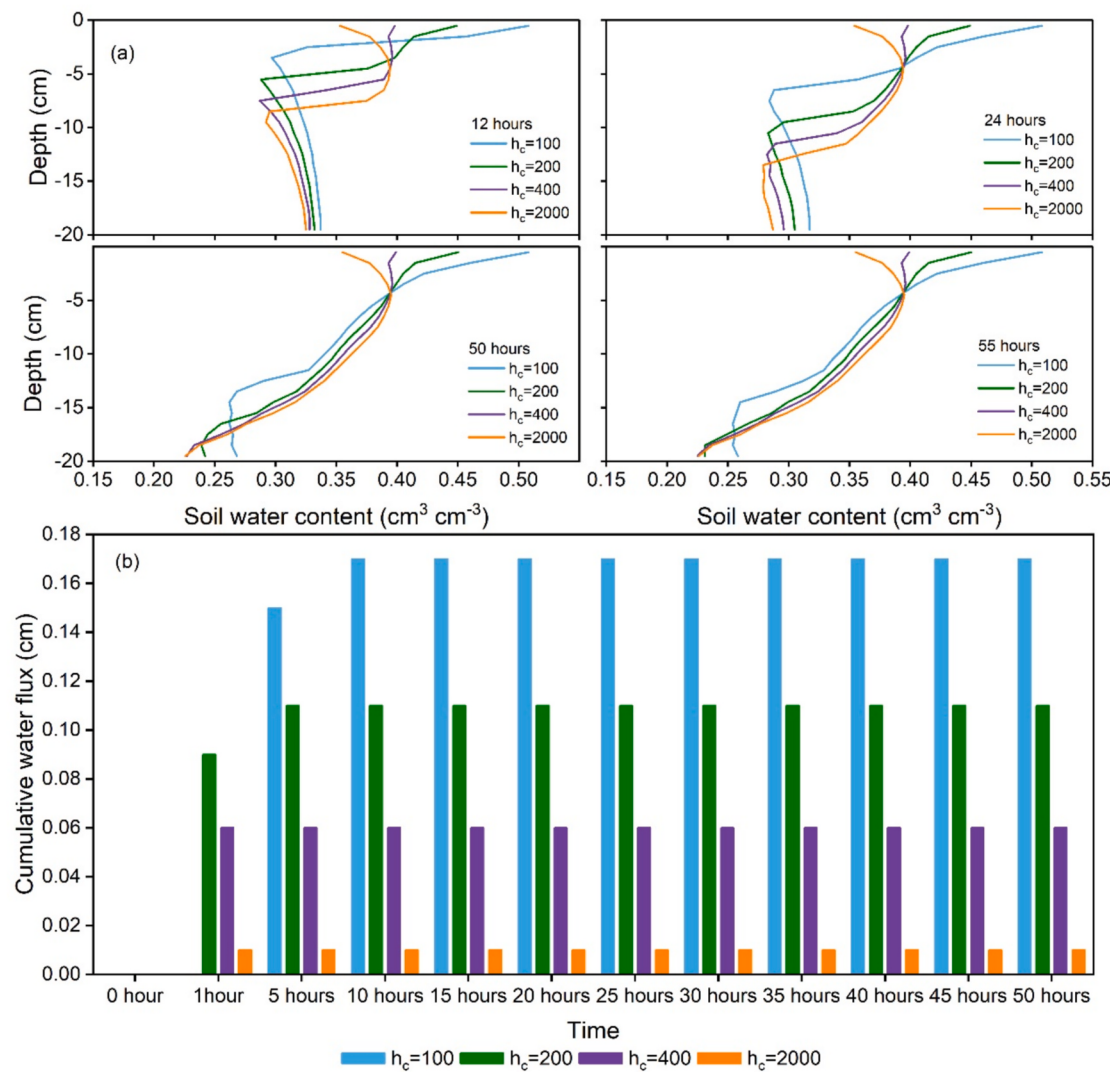


Fig. 4. Simulated total water contents (a) and cumulative water flux (b) for the surface layer (0–1 cm) at various h_c values after the freezing started. h_c represents the heat conductivity at the top boundary, $\text{J cm}^{-1} \text{°C}^{-1} \text{d}^{-1}$.

Table 2

Crop cultivation and irrigation scheduling at sunflower field during two agricultural years in Hetao.

Site	Year	Crop	Growth period (yyyy/mm/dd)	Irrigation			Mulching date (yyyy/mm/dd)
				Date (yyyy/mm/dd)	Event	Depth (mm)	
Hetao	2019–2020	Sunflower	2020/06/05–2020/09/20	2019/11/03	Pre-winter	150	2020/05/01
				2020/04/30	Pre-planting 1st	165	
				2020/05/28	Pre-planting 2nd	98	
				2020/06/23	Crop season 1st	40	
				2020/07/20	Crop season 2nd	90	
	2020–2021	Sunflower	2021/06/07–2021/09/23	2021/05/21	Pre-planting	175	2021/04/15
				2021/06/21	Crop season 1st	100	
				2021/07/19	Crop season 2nd	83	

Note: The salt concentration of irrigation water in the field site changes very little and averages 0.5 g L^{-1} .

year was divided into five periods: pre-freezing (P1), soil-freezing (P2), soil-thawing (P3), pre-planting (P4), and crop growth (P5) periods. The comparison of simulated and observed SWCs, C_{sw}, TWCS, and soil temperatures in the different periods of the root zone (0–60 cm) are presented in Figs. 6–8 for the calibration and validation periods, respectively. Meanwhile, the simulated and observed crop growth indicators (i.e., LAI and D-AGB) are shown in Fig. 9. The calibrated and validated soil hydraulic parameters and parameters related to soil heat, solute transport, surface mulching, and crop growth are listed in Table 1

and Table 3, respectively.

Results showed that the AHC-2.1R could reasonably reproduce the soil temperature dynamics during the calibration year (Fig. 8b), with RMSE = 3.10 °C , NSE = 0.93, R² = 0.95 (Table 4). The simulation of soil temperature depended on the setting of model parameters (such as soil thermal conductivity and heat capacity) and upper/bottom boundary conditions. It was also affected by the simulation of soil water flux. Since these factors were relatively complicated in field conditions, which may result in systematic biases for soil temperature simulation. The model

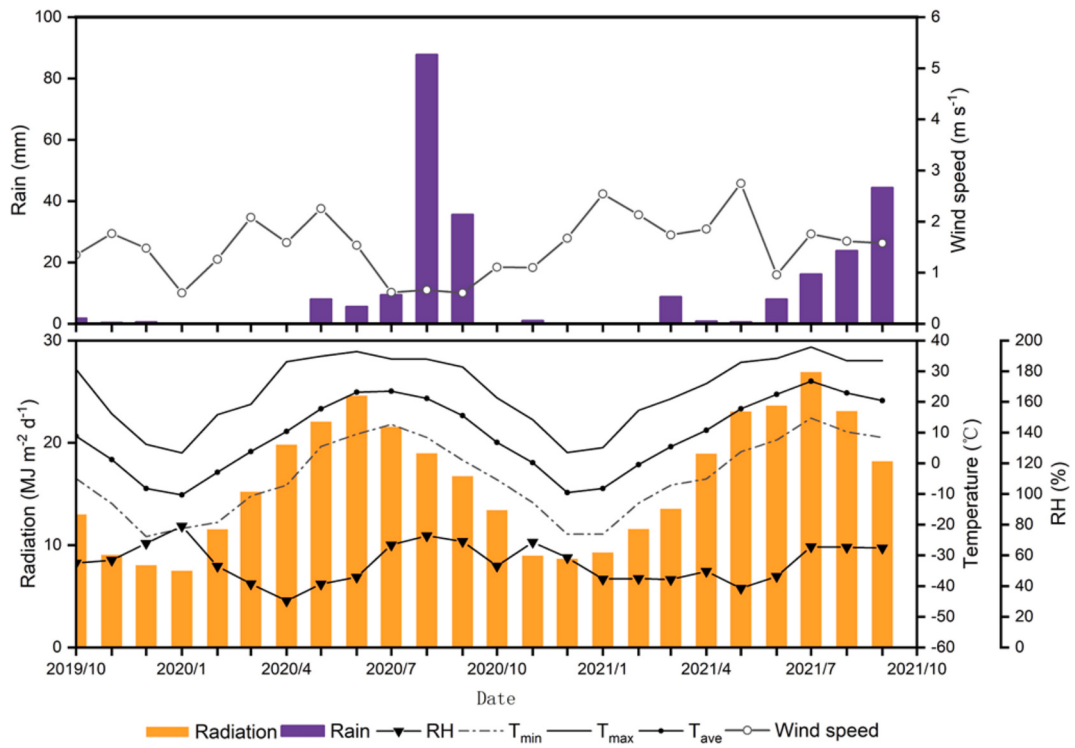


Fig. 5. Radiation, rainfall, relative humidity (RH), wind speed, average, maximum and minimum temperature (T_{ave} , T_{min} and T_{max}) at Linhe station during two agricultural years (Oct-2019 to Oct-2021).

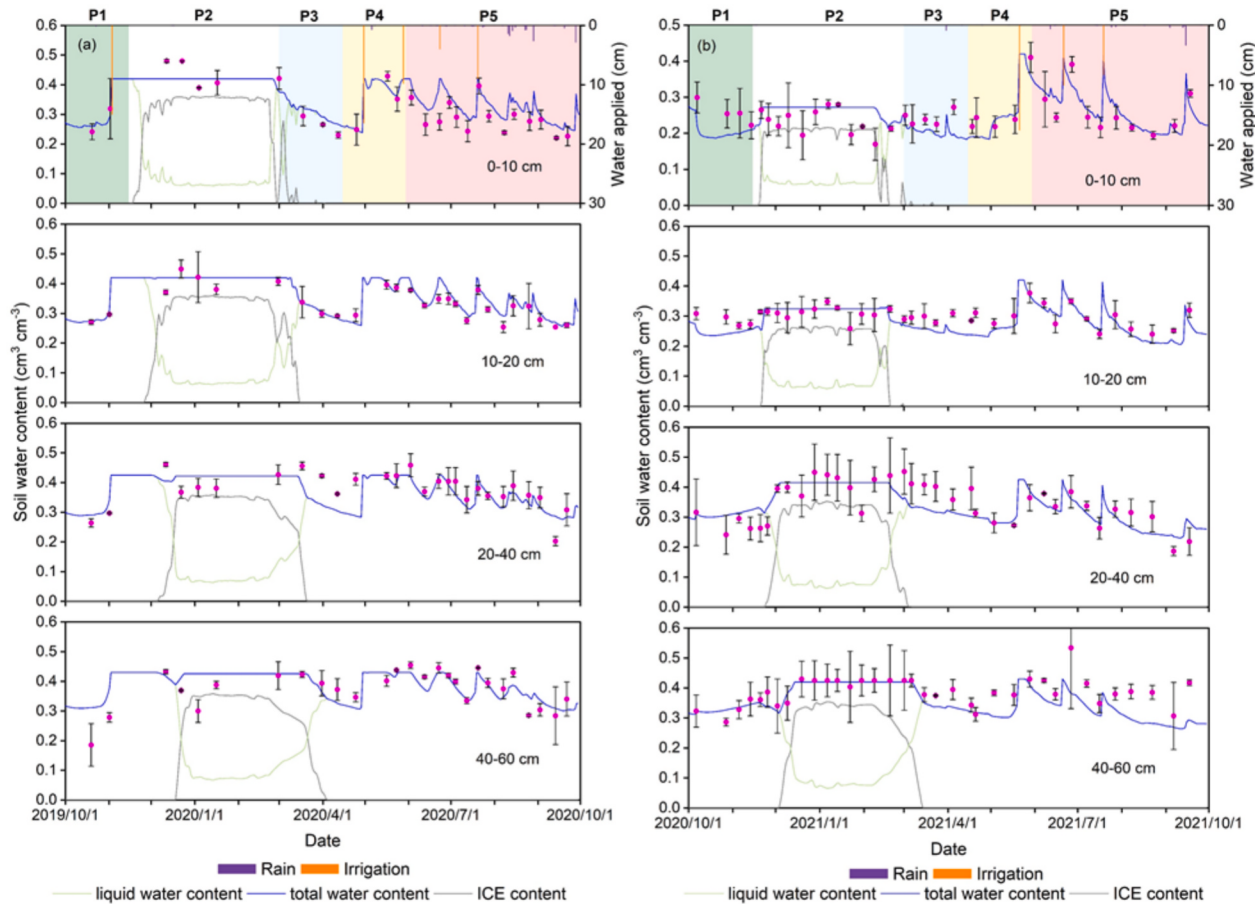


Fig. 6. Simulated total water contents (TWCs), liquid water contents and ice contents versus observed water contents in different layers during model calibration (a) and validation (b) for the field case. Points represent means \pm standard deviation.

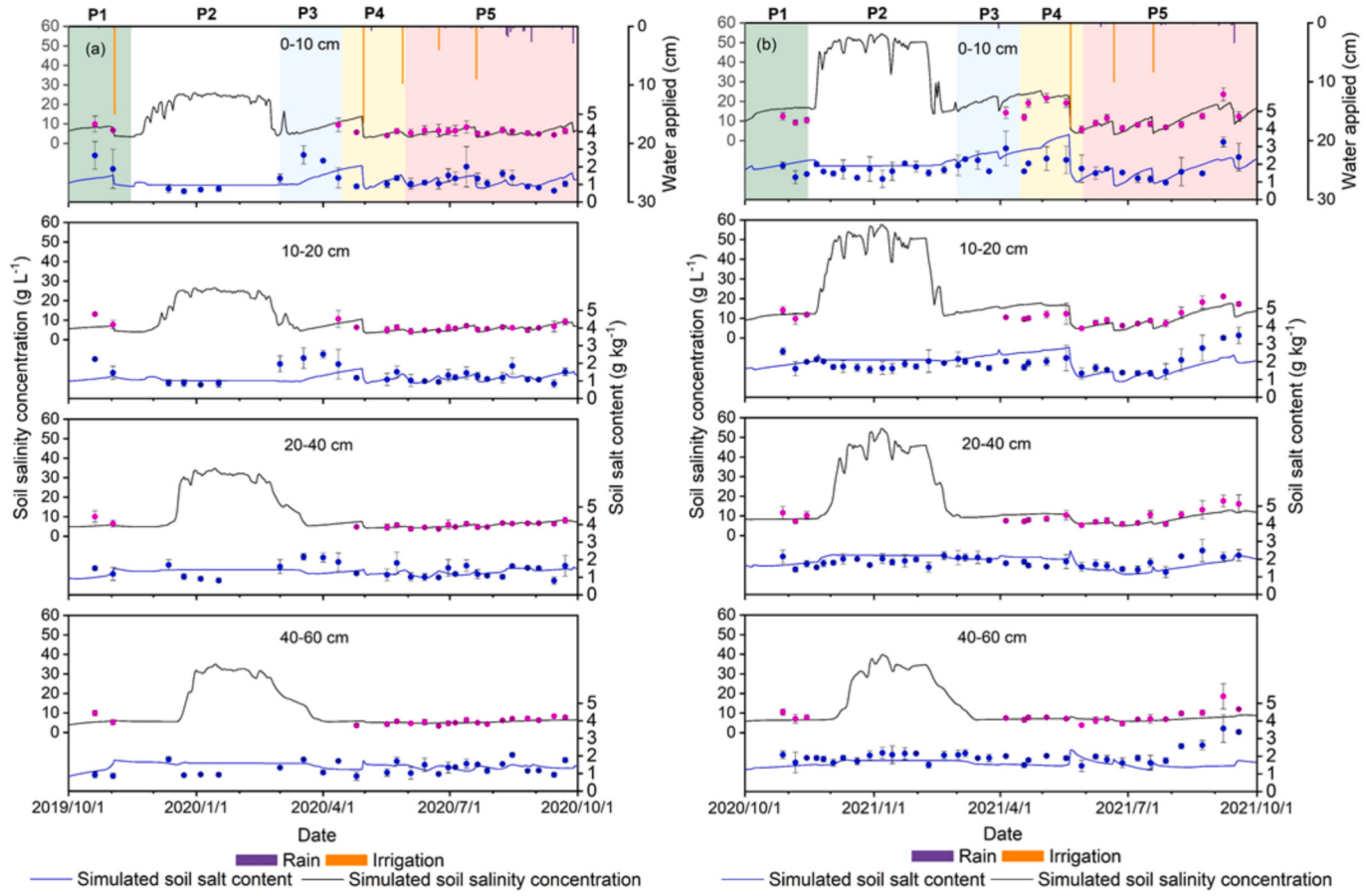


Fig. 7. Simulated versus measured soil salinity concentrations (C_{sw}) and soil salt contents (SSCs) in different layers during model calibration (a) and validation (b) for the field case. Points represent means \pm standard deviation.

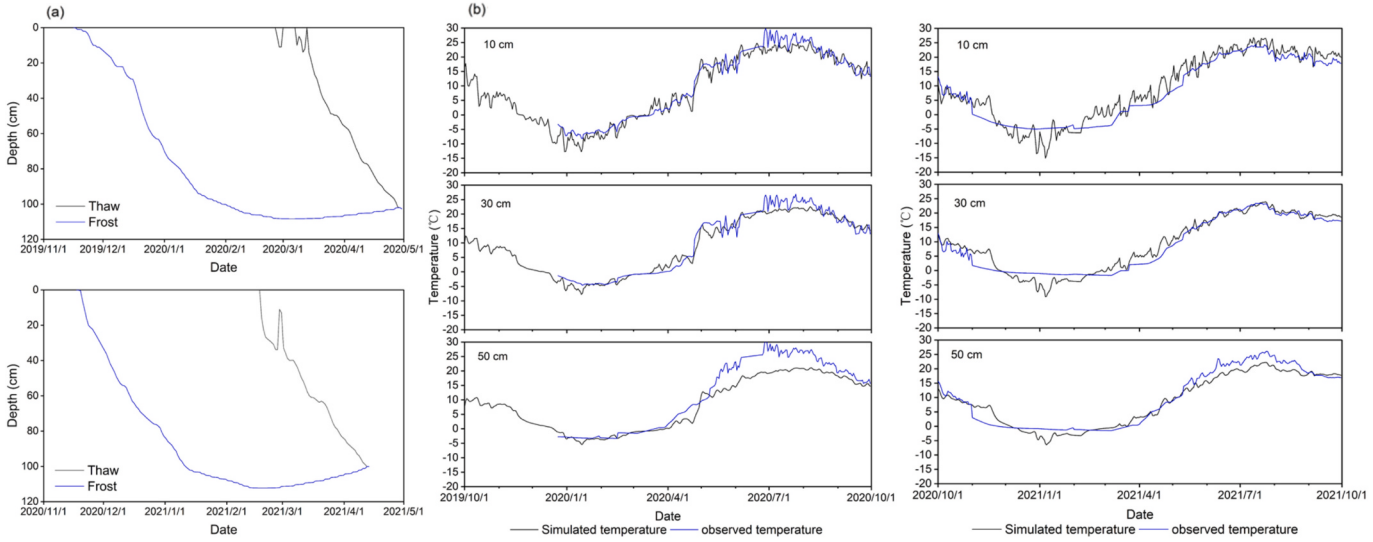


Fig. 8. Simulated soil freeze-thaw process (a) and soil temperatures (b) in different soil layers during model calibration and validation for the field case.

also showed a good performance in representing the dynamics of TWCs (Fig. 6a), with $\text{RMSE} = 0.04 \text{ cm}^3 \text{ cm}^{-3}$, $R^2 = 0.62$, and $\text{NSE} = 0.61$ (Table 4). For soil salinity simulation, the AHC-2.1R could reasonably represent the dynamics of C_{sw} and SSCs for different soil layers, both for soil freeze-thaw and other periods (Table 4 and Fig. 7). Note that the NSE value was slightly below zero for C_{sw} and SSCs, since the transport

mechanism of soil solution is more complicated than soil water. Additionally, soil salinity itself had strong spatial variability, and the measured values at each repeated sampling may also have certain differences (as can be seen from the error limit). Generally, the fitting index between the simulated and measured values is not as good as that for soil moisture (Xu et al., 2013; Ramos et al., 2023). In this case, the

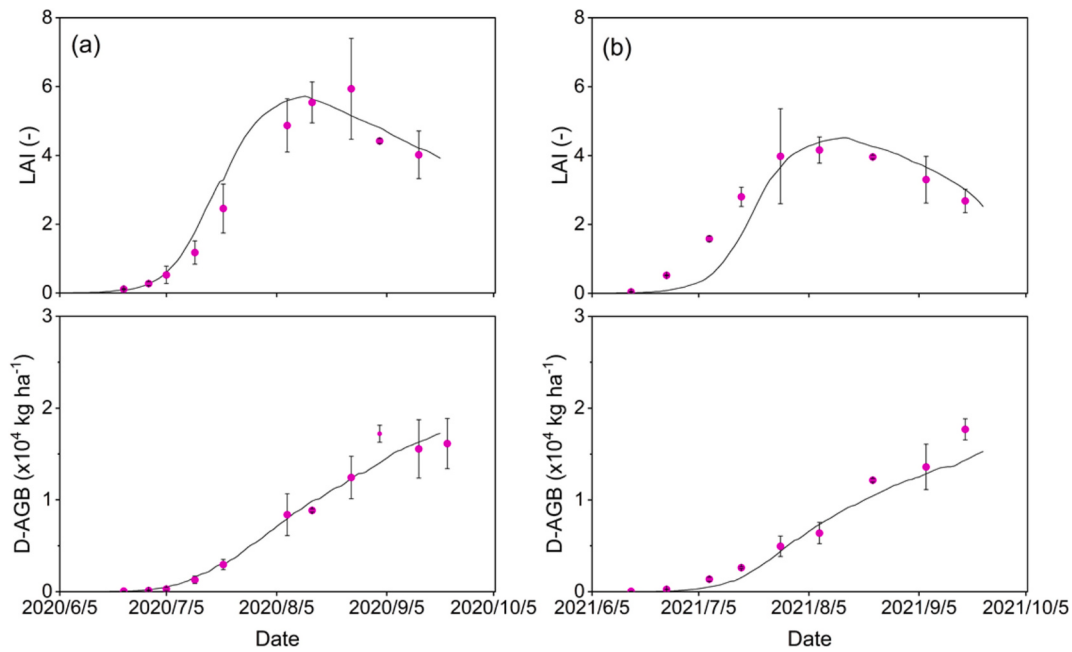


Fig. 9. Simulated and measured crop growth indicators (LAI and D-AGB) during two agricultural years (a: calibration, b: validation). D-AGB stands for dry above-ground biomass. Points represent means \pm standard deviation.

Table 3

Main calibrated parameters for heat transport, surface mulching, and crop growth in AHC-2.1R.

Process	Parameter	Meaning	Unit	Value
Heat transport	h_c	Heat conductivity of material on soil surface	$\text{J cm}^{-1} \text{ °C}^{-1} \text{ day}^{-1}$	70
Surface mulching	c_{mul}	Fraction of surface covered by mulch	—	0.55
	f_{mm}	Adjusted factor for mulch material	—	1
Crop growth	CH_{max}^*	Maximum crop/canopy height	cm	260/250
	LAI_{max}^*	Potential maximum LAI	—	6.2/4.8
	RD_{max}	Maximum root depth	cm	60
	TBA	Base temperature for temperature growth	°C	6
	$TOPT$	Optimal temperature for crop growth	°C	25
	$RUEP^*$	Potential plant radiation use efficiency at 330 ppm CO ₂	(kg ha ⁻¹) (MJ m^{-2}) ⁻¹	39/41
	$FDLAI$	Fraction of growing season when LAI declines	—	0.65
	PHU^*	Total heat units required for plant maturity	°C	1850/1900
	HI	Potential harvest index at maturity	—	0.3

Note: * indicates different parameter values for variety differences in the two agricultural years.

simulation results could still reasonably capture the dynamics of C_{sw} and SSCs and reflect the leaching and accumulation trends of salt in different soil layers. For crop growth, the simulated LAI and D-AGB agreed well with the observation (Fig. 9a), with RMSE values equal of 0.49 and 1.1 t ha⁻¹, respectively, and R² values greater than 0.95 (Table 4). The simulated crop yield in 2020 was 4.74 t ha⁻¹, which was slightly higher

Table 4

Goodness of fit indicators relative to model calibration and validation.

	Items	MRE (%)	NSE	R ²	RMSE
Calibration	Soil water content (cm ³ cm ⁻³)	3.83	0.61	0.62	0.04
	Soil salinity concentration (g L ⁻¹)	-0.39	-0.07	0.22	1.80
	Soil salt content (g kg ⁻¹)	4.91	-0.09	0.03	0.47
	Soil temperature (°C)	16.29	0.93	0.95	3.10
	LAI (—)	9.61	0.95	0.96	0.49
	D-AGB (t ha ⁻¹)	21.01	0.97	0.97	1.1
Validation	Soil water content (cm ³ cm ⁻³)	-2.69	0.61	0.65	0.05
	Soil salinity concentration (g L ⁻¹)	4.07	0.29	0.49	3.59
	Soil salt content (g kg ⁻¹)	2.8	-0.49	0.04	0.54
	Soil temperature (°C)	-2.62	0.92	0.92	2.79
	LAI (—)	-11.34	0.45	0.87	0.64
	D-AGB (t ha ⁻¹)	-19.65	0.92	0.97	1.59

Note: MRE, mean relative error; RMSE, root mean square error; NSE, Nash and Sutcliffe model efficiency; R², coefficient of determination; LAI, leaf area index; D-AGB, dry above-ground biomass.

than the observed value (4.7 t ha⁻¹).

All calibrated parameters were used as model inputs during validation except several parameters that were affected by field management practices and the variety differences of crops during the two years. Meanwhile, some crop parameters (CH_{max} , LAI_{max} , $RUEP$, and PHU) were adjusted during the two agr-years due to the crop variety (CH_{max} , $RUEP$, and PHU) and based on field observation (i.e., LAI_{max}) (Table 3). Validation results showed that the simulated SWCs were in good agreement with the observed values with RMSE = 0.05 cm³ cm⁻³, R² = 0.65, and NSE = 0.61 (Table 4). Meanwhile, the simulated soil temperature matched well with the monitored one during validation with RMSE = 2.79 °C, R² = 0.92, and NSE = 0.92 (Fig. 8b and Table 4). Moreover, the simulated C_{sw} and SSCs were in reasonable values of each

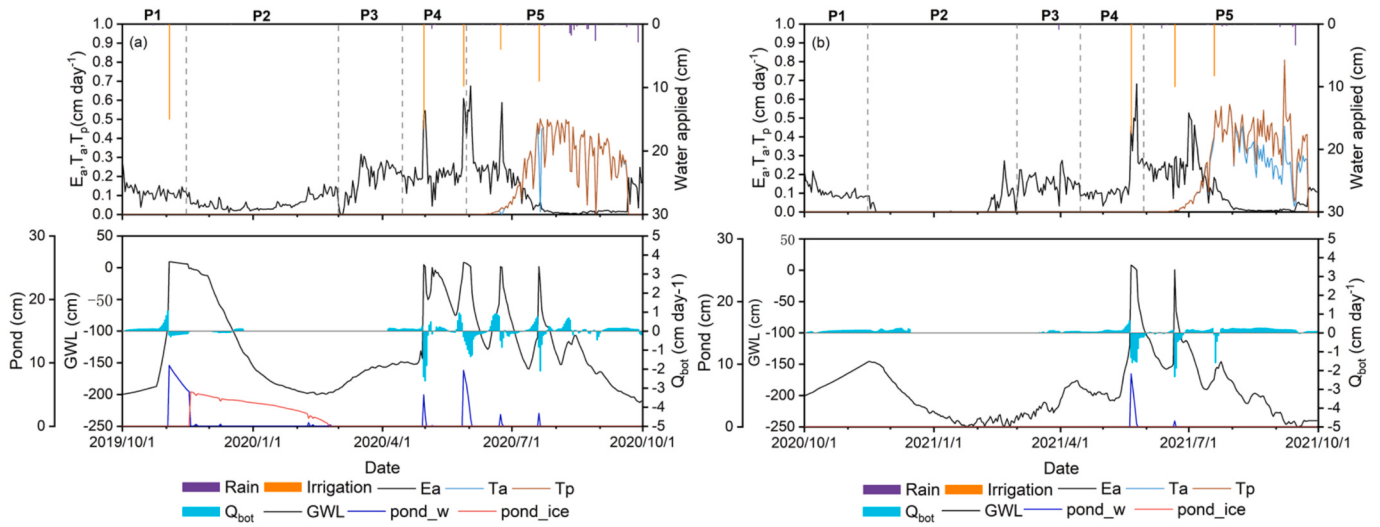


Fig. 10. Actual soil evaporation (E_a), crop potential (T_p) and actual transpiration (T_a) and bottom vertical fluxes (Q_{bot}) at the root zone (60 cm) versus irrigation, rainfall and groundwater level (GWL) in two agricultural years (a: calibration, b: validation).

fitting indicator. The simulated LAI and D-AGB also agreed well with the measured values (Fig. 9b and Table 4), and the simulated crop yield was 4.56 t ha⁻¹, close to the measured values of 4.6 t ha⁻¹.

In addition, the unidirectional freezing and the bi-directional thawing process of the seasonal frozen and thawed soil (Fig. 8a) were well captured by AHC-2.1R, which was also similar to previous studies (Xun et al., 2022; Liu et al., 2024; Hu et al., 2023). In summary, the general agreement between the simulated and observed data showed that the AHC-2.1R could reasonably represent the dynamics of SWCs, temperatures, and SSCs, and the process of crop growth and yield formation over the two entire agr-years in this seasonally frozen region.

(2) Simulation analysis and evaluation

Results showed that AHC-2.1R reasonably simulated the soil water and salt dynamics during the freeze-thaw period (P2 and P3) and provided quantitative explanations for these complicated processes (Figs. 6–10). For the first agr-year (2019–2020), the groundwater level (GWL) had already risen before autumn irrigation, primarily due to the influence of surrounding agricultural irrigation (e.g., lateral groundwater flow). Following the application of autumn irrigation (150 mm on Nov 3rd), the GWL rose rapidly, leading to near-saturation of the entire soil profile and surface water ponding. Moreover, the poor drainage conditions weakened the leaching effect of autumn irrigation (Fig. 11a). During the subsequent soil freezing period (P2, from Nov 16th to Mar 1st), the uninfiltated ponding water was frozen into the ice layer at the soil surface, which maintained a certain amount of surface evaporation through sublimation (Fig. 10a). Meanwhile, the upper soil layers gradually froze, presenting an instability phenomenon of freeze and thaw cycles (Fig. 6a). Under the influence of the negative air temperature, the freezing depth increased progressively and eventually reached a maximum depth of 110–120 cm (Fig. 8a).

However, as the soil profile was nearly saturated due to autumn irrigation, the upward migration of soil water toward the freezing front was minimal (8.6 mm during P2) (Table 5). When entering the soil thawing period (P3), the soil thawed bi-directionally (Fig. 8a), driven by air temperature and bottom heat flux. During this period, intense soil evaporation (2–3 mm d⁻¹) (Fig. 10a) led to a gradual decrease in soil

water content within the profile (Fig. 6a). Simulations also indicated that there was an alternating phenomenon of freezing and thawing in the early stage of melting, causing significant fluctuations in C_{sw} (Figs. 6a and 6a).

Overall, AHC-2.1R effectively captured the soil freeze-thaw dynamics during the first agr-year. However, the field conditions of the second agr-year during the freeze-thaw period were significantly different from the first agr-year, due to land restoration and the absence of autumn irrigation. Despite that, AHC-2.1R was able to simulate the actual soil water and salt dynamics accurately. Because no autumn irrigation was applied during P1 in the second agr-year, soil water content remained relatively low until early P2 (Fig. 6b). During soil freezing, driven by the soil water potential gradient, water gradually migrated upward from the unfrozen soil layers to the frozen surface layer, causing the TWCSs of 0–60 cm layer to approach saturation. Subsequently, once the profile reached saturation or the ice contents became large enough, the soil water flux at 60 cm depth was decreased to zero (Fig. 10b). AHC-2.1R accurately captured the complex upward migration of water and salt during soil freezing. Additionally, the treatment of limiting full saturation efficiently prevented the total soil water content from exceeding θ_s during the freezing period, effectively ensuring the model's numerical stability. Moreover, due to soil compaction caused by large machinery during field restoration in the early P1, both the θ_s and k_s values decreased. This resulted in lower water content in the 0–20 cm surface soil after freezing during P2 (approximately 0.1 cm³ cm⁻³ lower than in the first agr-year). By adopting the phase-specific θ_s and k_s settings, AHC-2.1R could represent the impact of soil compaction on soil water and salt processes during the freezing period. Throughout the freezing period, the absence of autumn irrigation led to higher salt storage in the root zone in the second agr-year, i.e., about 60 mg cm⁻² greater than in the first agr-year (increased by 50%) (Fig. 11).

During P4 and P5 periods, the salt storage was highly correlated with the field irrigation. Pre-planting irrigation effectively leached salts from the root zone, reducing salt storage by 25 % and 36 % in two agr-years, respectively, thereby providing favorable water-salt conditions for seed germination (Fig. 11). During the crop growth season, salt storage decreased rapidly after irrigation but exhibited the opposite trend

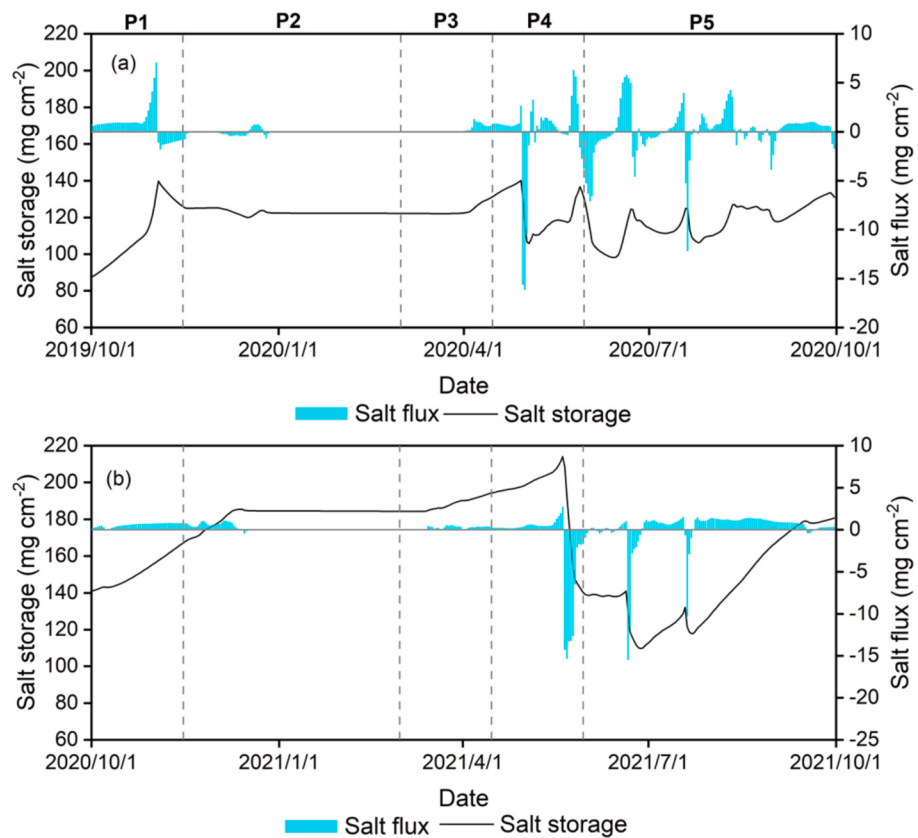


Fig. 11. Variations of salt storage in the 0–60 cm soil profile and daily vertical salt flux (positive for upward) at 60 cm soil depth during two agricultural years (a: calibration, b: validation).

Table 5

Water balance components (mm) in the root zone (i.e., 0–60 cm) in different periods over two agricultural years in Hetao case.

Year	Date (m/d)	Precipitation	Irrigation	Evaporation	Transpiration	Percolation	Capillary rise	Water storage
2019–2020	Initial	—	—	—	—	—	—	182.7
	P1: 10/1–11/15	2.2	150	55.8	0	26.1	60.8	313.8
	P2: 11/16–3/1	0.6	0	61.8	0	13.6	8.6	247.6
	P3: 3/2–4/15	0	0	84.3	0	0	13.9	177.1
	P4: 4/16–5/30	8	263	110.5	0	90.0	67.6	315.6
	P5: 5/31–9/20	109	130	114.8	254.4	146.4	153.9	193.0
2020–2021	Initial	—	—	—	—	—	—	181.8
	P1: 10/1–11/15	0	0	49.1	0	0.3	48.5	180.9
	P2: 11/16–3/1	1	0	21	0	0	46.9	207.8
	P3: 3/2–4/15	9.4	0	70.24	0	0.02	21.5	168.5
	P4: 4/16–5/30	0.8	175	71.9	0	92.5	48.0	227.9
	P5: 5/31–9/23	60.8	183	136.3	240.3	86.5	153.9	162.1

during irrigation intervals. Additionally, in the first agr-year, crop growth experienced several times of water stress due to waterlogging during irrigation events (Fig. 12a). Furthermore, the temperature stress was dominant during the early and late stages of the crop growth period. In other stages, water-salt stress played a more significant role. Especially in 2021, water-salt stress was more severe (with an average water-salt stress factor of 0.71), particularly during the late growth stage (Fig. 12b). This is mainly due to the non-application of autumn irrigation and less rainfall and irrigation during the growth season.

Overall, simulation results of AHC-2.1R during the freeze-thaw

periods of the two agr-years showed a similar trend to the classical SHAW and its modified version (SHAW-SC) (Xun et al., 2022; Liu et al., 2024). However, differences were observed in crop water consumption and crop stress during the crop growth season due to differences in the calculation principles for evapotranspiration and water stress. Therefore, the AHC-2.1R can effectively capture soil water and salt dynamics, soil temperature distribution, and crop growth processes over the entire agr-year.

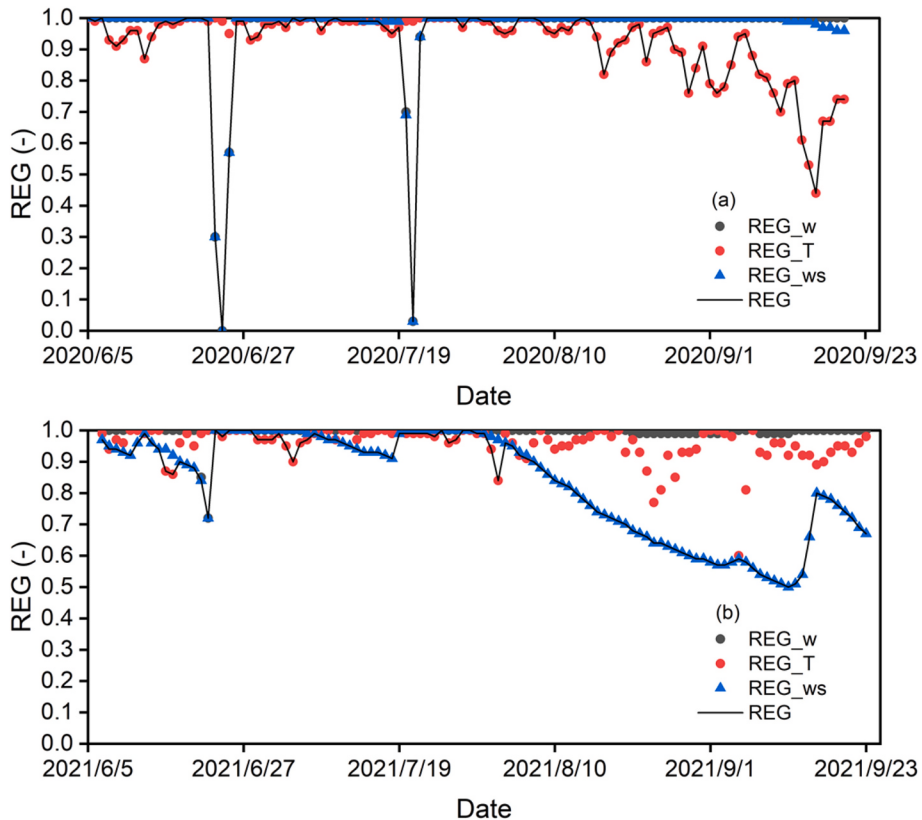


Fig. 12. Daily water stress factor (REG w), temperature stress factor (REG T), water-salinity stress factor (REG ws), and the total stress factor (REG) during crop growth periods in 2020 and 2021 (a: calibration, b: validation).

4. Discussion

Compared to the original AHC-2.0, the AHC-2.1R significantly enhanced the modeling capability during the soil freeze-thaw periods. Figs. A1–A3 presented the differences in the simulation of annual water-salt dynamics between the original and improved models. As mentioned earlier, AHC-2.0 employed relatively simple approaches to describe soil water-heat coupling and used a correction factor to reduce soil hydraulic conductivity. Consequently, the AHC-2.0 cannot adequately simulate upward soil water migration caused by surface soil freezing and the significant increase in soil salinity concentration due to phase change from liquid water to ice (Figs. A2, A3). Once the soil has completely thawed (P4 period), excessive irrigation during this period saturated the soil profile, reducing the discrepancy between the two models in water and salt simulation (Fig. A2). However, for early-sown crops (e.g., spring wheat and spring maize), the period from mid-to-late March to April corresponded to the sowing and seedling stage. Accurate characterization of soil water-salt conditions was essential for evaluating crop emergence rate and seedling growth and ensuring the accuracy of subsequent simulation. The original model, due to its oversimplified treatment of the freeze-thaw process, underestimated the soil water content and overestimated soil salinity concentration in scenario cases (Figs. A2, A3). Moreover, during the P2, groundwater moves upward to recharge the upper soil layer under the influence of soil water potential gradient caused by soil freezing; whereas, the melted water recharges the groundwater during the P3 (Fig. A4). The interaction between groundwater and soil water during the freezing and thawing period is well reflected by AHC-2.1R, which is consistent with the previous

experimental research (e.g., Wu et al. (2023)). However, there is almost no interaction occurring between groundwater and soil water in simulation using AHC-2.0, due to its over-simplification of the freeze-thaw process. All these highlighted the necessity of improving the soil freeze-thaw functions for the agro-ecosystem models.

Regarding the impact of human agricultural activities on soils, the AHC-2.1R dynamically adjusted soil hydraulic parameters, enabling it to more accurately reflect the effects of mechanical compaction on soil water-salt dynamics (Fig. 6b). Moreover, the model incorporated an energy-based correction for apparent heat capacity (when temperatures cross the freezing point) and restricted the net water flux inflow into nodes to improve numerical stability and computational efficiency. The energy-based correction reduced the number of iterations and allowed the use of larger time step, effectively improving the calculation efficiency. Such as, for the field case of the second agr-year (2020–2021), if we adopted the energy-based correction, the simulation time and the total number of iterations were only 167.94 s and 201,465 times, respectively. However, if the energy-based correction was not used, this simulation test needed 1090.45 s and 1,187,601 iterations. Furthermore, restricting the net water flux into nodes could prevent the TWC from exceeding the saturated water content in the freezing period, further enhancing the model's stability. Field case simulation indicated that if the treatment of restricting the net water flux into nodes was not employed, the simulated TWC would be greater than θ_s under freezing conditions, subsequently resulting in the non-convergence problem and interruption in numerical calculation. The two treatments were similar to those in the SHAW model (Flerchinger and Saxton, 1989), allowing the upgraded model to address instability and inefficiency caused by

water-heat coupling and water–ice phase transitions.

Moreover, the AHC-2.1R adopted a simultaneous iteration procedure of soil freeze–thaw process and achieved fully coupled simulations for cold-region farmlands, which offers significant advantages compared to the hybrid use of different models (e.g., Li et al., 2012; Liu et al., 2024). It also had some advantages in calculation efficiency or simulation functions compared to the other models that also took the freeze–thaw process into account. Such as, HYDRUS-1D used two loop iterations in the water-heat coupling, and may cause instability at saturation (Šimůnek et al., 2016; Zheng et al., 2021); AHC-2.1R had a comprehensive solute transport and transformation module based on chain ADE, while CoupModel provided a simplified solute module with only considering the convection effects; and AHC-2.1R also included the simulation for the fate of carbon and nitrogen and the detailed crop growth compared to SHAW. Furthermore, as AHC-2.0 has already provided comprehensive computational functions (including soil water-heat-solute transport, soil nitrogen and carbon turnover, gas emissions, and crop growth functions) and field management capabilities (e.g., irrigation scheduling and lateral drainage design), the improvements in soil freeze–thaw simulation largely strengthen its simulation capacity and applicability in seasonal frozen regions. However, the current model still simplifies the energy exchange at the upper boundary. Future developments may focus on incorporating energy balance methods to strengthen the quantitative representation of upper heat boundary conditions and introducing descriptions of soil frost heave to accurately capture its effects on soil freezing.

5. Summary and conclusion

We presented the development of the improved AHC model (i.e., AHC-2.1R) to enhance the frost simulation capabilities of existing agro-ecosystem models and the applicability in seasonal frozen regions. The new upgraded calculation principles and efficient numerical method were introduced to realize a coupled, simultaneous simulation of soil water–vapor–heat transport, solute transfer, and crop growth over an agricultural year (agr-year, including crop growth season and soil freeze–thaw period). The significant modifications were conducted based on the previous version of AHC-2.0, mainly including (1) employing the modified Richards equation and heat transport equation, providing new functions for considering vapor transfer and soil freeze–thaw processes; (2) upgrading the numerical method with Newton–Raphson technique and reconstructing the numerical iteration procedures to solve the water-heat equations under soil frozen conditions simultaneously; (3) proposing two special treatments (i.e., the limitation of net water flux and the available energy-based method for a phase change) that can specifically improve the stability of water-heat numerical calculations during freeze–thaw periods; and (4) incorporating a new snowpack module to calculate the snow accumulation and snowmelt, with less data requirement. The improved AHC-2.1R was first well-tested by the experimental dataset from a typical soil column freezing test. Then, it was further calibrated and validated with detailed field experimental data from sunflower field experiments over two entire agr-years in the Hetao Irrigation District (Hetao) of the upper Yellow River basin.

The experimental soil column test indicated that the AHC-2.1R could accurately capture the soil water-heat coupling process during soil freezing, with a good agreement between the measured and simulated total water contents and soil temperatures. Meanwhile, the sensitivity test further demonstrated the rationality of the model. Particularly, simulation results indicated that the model stability treatment (based on the available energy method) effectively ensured numerical stability and computational efficiency during soil freezing conditions. The field case simulation of two entire agr-years showed that the AHC-2.1R could reasonably simulate the dynamics of layered soil water contents, salinity concentration, temperature, and crop growth, with acceptable fitting indicators between simulation and observation. The accuracy of hydrothermal simulation during the freeze–thaw period has been significantly improved with AHC-2.1R, compared to the original AHC-2.0. In particular, the field test demonstrated that the other model stability treatment (i.e., the limitation of net water flux) effectively maintained the stability of numerical calculations for a full saturation state during the soil freezing process. Moreover, the field scenario analysis with deep groundwater depth further demonstrated the necessity of considering the soil freeze–thaw process.

In conclusion, the model improvements have effectively enhanced the simulation and prediction capabilities of the agro-ecosystem models during the soil freeze–thaw period. The improved AHC-2.1R could be more reliably applied to support farmland water-salt-carbon–nitrogen management and crop production for seasonal frozen regions. Follow-up investigations may focus primarily on improving the calculation of surface energy balance and the description of frost heave effects.

CRediT authorship contribution statement

Yutao Liu: Writing – review & editing, Writing – original draft, Software, Methodology, Investigation, Formal analysis, Conceptualization. **Xu Xu:** Writing – review & editing, Writing – original draft, Supervision, Software, Resources, Methodology, Funding acquisition, Conceptualization. **Yihao Xun:** Writing – review & editing, Investigation, Data curation. **Chen Sun:** Writing – review & editing, Supervision, Conceptualization. **Guanhua Huang:** Supervision, Resources, Software, Funding acquisition.

Declaration of competing interest

The authors declare that they have no known competing financial interests or personal relationships that could have appeared to influence the work reported in this paper.

Acknowledgments

This research was supported by the 14th Five-year National Key Research and Development Program of the Chinese Ministry of Science and Technology (grant number: 2024YFD1700400), the National Natural Science Foundation of China (grant numbers: 52379053 and 52022108), and the Key Research Project of Science and Technology in Inner Mongolia Autonomous Region of China (grant numbers: NMKJXM202208 and NMKJXM202301).

Appendix A. Some equations used in different versions of AHC model

Equation	Reference/source
$\frac{\partial \theta}{\partial t} = C_w(h) \frac{\partial h}{\partial t} = \frac{\partial}{\partial z} \left[K(h) \left(\frac{\partial h}{\partial z} + 1 \right) \right] - S_w(h)$	(A1) [#] Xu et al. (2018)
$\frac{\partial C_s(\theta) T}{\partial t} = \frac{\partial}{\partial z} \left[\lambda(\theta) \frac{\partial T}{\partial z} \right] - \rho_l C_l \frac{\partial q_l T}{\partial z} - S_h$	(A2) [#] Xu et al. (2018)
$\frac{\partial (\theta c_1 + \rho_b Q_1)}{\partial t} = - \frac{\partial q c_1}{\partial z} + \frac{\partial}{\partial z} \left[\theta (D_{dif,1} + D_{dis,1}) \frac{\partial c_1}{\partial z} \right] - \left(\mu_{w,1} + \mu'_{w,1} \right) \theta c_1 - \left(\mu_{s,1} + \mu'_{s,1} \right) \rho_b Q_1 - K_{r,1} S c_1 (k=1)$	(A3) [#] Xu et al. (2018)
$\frac{\partial}{\partial z} \left[\theta (D_{dif,1} + D_{dis,1}) \frac{\partial c_1}{\partial z} \right] - \left(\mu_{w,1} + \mu'_{w,1} \right) \theta c_1 - \left(\mu_{s,1} + \mu'_{s,1} \right) \rho_b Q_1 - K_{r,1} S c_1 (k=1)$	(A4) This study
$q_v = -D_v \frac{\partial \rho_v}{\partial z} = -D_v \left(h_s s_v \frac{\partial T}{\partial z} + \zeta \rho_{vs} \frac{\partial h_v}{\partial z} \right)$	(A5) van Genuchten (1980)
$S_e(h) = \frac{\theta(h) - \theta_r}{\theta_s - \theta_r} = \frac{1}{(1 + \alpha_l h ^n)^{1-1/n}}$	(A6) Mualem (1976)
$K(h) = K_s S_e^{i_p} \left[1 - \left(1 - S_e^{i/(n-1)} \right)^{(n-1)/n} \right]^2$	(A7) [#] De Vries (1963)
$C_s = f_{sand} C_{sand} + f_{clay} C_{clay} + f_{organic} C_{organic} + \theta C_{water} + f_{air} C_{air}$	(A8) [#] De Vries (1963)
$\lambda = \frac{k_w \theta \lambda_w + k_a \sigma_a \lambda_a + \sum_{i=1}^4 k_i \sigma_i \lambda_i}{k_w \theta + k_a \sigma_a + \sum_{i=1}^4 k_i \sigma_i}$ (without ice in solid parts)	(A9) Kirkham and Powers (1972)
$T_{atm} = \bar{T} + A_{mp} \sin \left(\frac{2\pi t}{p_t} - \frac{7\pi}{12} \right)$	(A10) Hillel (1998)
$h_{so} = -100 \frac{i_c M R T_k}{\rho g} = -100 \frac{i_c R T_k}{\rho g} \frac{c}{M}$	(A11) Kustas et al. (1994)
$q_{melt} = C(T_{av} - T_b)$	(A12) Fernández (1998)
$q_{melt,r} = \frac{P_r C_{ww} (T_{av} - T_{snow})}{L_m}$	(A13) This study
$(\theta_i^{j+1} - \theta_i^j) + \frac{\rho_l}{\rho_l} (a_i^{j+1} - a_i^j) = \frac{\Delta t}{\Delta z_i} \left(K_{i-1/2}^{j+1} \frac{h_{i-1}^{j+1} - h_i^{j+1}}{\Delta z_u} + K_{i-1/2}^{j+1} - K_{i+1/2}^{j+1} \frac{h_i^{j+1} - h_{i+1}^{j+1}}{\Delta z_L} - K_{i+1/2}^{j+1} \right)$	(A14) This study
$\frac{C_s^{j+1} T_{i-1}^{j+1} - C_s^j T_i^j}{\Delta t} - L_f \rho_i \frac{a_i^{j+1} - a_i^j}{\Delta t} + L_v \frac{\partial \rho_v}{\partial T} \frac{T_i^{j+1} - T_i^j}{\Delta t} + L_v \frac{q_{v,i-1/2}^{j+1} - q_{v,i+1/2}^{j+1}}{\Delta z_i} = \frac{1}{\Delta z_i} \left(\lambda_{i-1/2}^{j+1} \frac{T_{i-1}^{j+1} - T_i^{j+1}}{\Delta z_u} - \lambda_{i+1/2}^{j+1} \frac{T_i^{j+1} - T_{i+1}^{j+1}}{\Delta z_L} \right)$	(A15) This study
$-\rho_L C_l \frac{q_{l,i-1/2}^{j+1} (T_{i-1}^{j+1} + T_i^{j+1}) / 2 + \rho_L C_l \frac{q_{l,i+1/2}^{j+1} (T_i^{j+1} + T_{i+1}^{j+1}) / 2}{\Delta z_i} - c_v \frac{q_{v,i-1/2}^{j+1} (T_{i-1}^{j+1} + T_i^{j+1}) / 2}{\Delta z_i} + c_v \frac{q_{v,i+1/2}^{j+1} (T_i^{j+1} + T_{i+1}^{j+1}) / 2}{\Delta z_i} - S_{h,i} - \rho_L C_l S_{w,i} T_{w,i}^j}{\Delta z_i}$	(A16) Campbell (1985) Hansson et al. (2004)
$\lambda(\theta) = \lambda_0(\theta) + \beta_\ell C_w q_w $	(A17) Xu et al. (2018)
$\lambda_0(\theta) = C_1 + C_2(\theta + F\theta_l) - (C_1 - C_4) \exp \left\{ - [C_3(\theta + F\theta_l)]^{C_5} \right\}$	
$C_w(h) = \frac{\left(1 - \frac{1}{n}\right) \cdot \alpha_l \cdot n \cdot \alpha_l h ^{n-1} (\theta_s - \theta_r)}{(1 + \alpha_l h ^n)^{2n-1/n}}$	

Note: the superscript [#] indicates the equation is only used in AHC-2.0 but is no longer used in AHC-2.1R.

The additional explanation of variables:

S_e is the effective saturation, θ is the soil water content ($\text{cm}^3 \text{ cm}^{-3}$), θ_r and θ_s denote the residual and saturated water contents ($\text{cm}^3 \text{ cm}^{-3}$), respectively, K_s is the saturated hydraulic conductivity (cm d^{-1}), a_l (cm^{-1}) and n (–) are empirical shape parameters, and λ_p is a pore connectivity/tortuosity parameter (–), Q_k is the amount absorbed in soil particles (g g^{-1}), the subscripts w and s refer to liquid and solid phases, respectively, and the subscript k represents the k^{th} chain number, μ is the first-order rate coefficient of transformation (d^{-1}), μ' is the similar first-order rate coefficient of transformation providing connections between individual chain species, D_v is vapor diffusivity in the soil ($\text{cm}^2 \text{ d}^{-1}$), \bar{T} is the daily average temperature near the soil surface (or atmospheric air) ($^{\circ}\text{C}$), A_{mp} is the amplitude of the sine wave ($^{\circ}\text{C}$), and p_t is a period of time (d) necessary to complete one cycle of the sine wave (taken to be 1 day). c_M is the molar concentration of the solute in the solution (mol L^{-1}), R is the universal gas constant ($8.3143 \text{ J mol}^{-1} \text{ K}^{-1}$), T_k is the temperature of the soil in Kelvin (K), g is the gravitational acceleration (9.81 m s^{-2}), and M is the molecular weight of specific solute (g mol^{-1}). C is a ‘degree-day’ factor ($\text{cm } ^{\circ}\text{C}^{-1} \text{ d}^{-1}$), T_{av} is the daily average temperature ($^{\circ}\text{C}$), T_b is the base temperature ($^{\circ}\text{C}$), P_r is rainfall (cm d^{-1}), C_{ww} is the heat capacity of water ($\text{J kg}^{-1} ^{\circ}\text{C}^{-1}$), T_{snow} is the temperature of the snowpack, which is set to $0 ^{\circ}\text{C}$, L_m is latent heat of fusion ($333,580 \text{ J kg}^{-1}$), C_T is the derivation of θ_l with respect to T , $\lambda_0(\theta)$ is the thermal conductivity of the porous medium (solid plus water) in the absence of flow ($\text{W m}^{-1} \text{ K}^{-1}$), β_t is longitudinal thermal dispersivity (L), and C_i ($i = 1, \dots, 5$) are constants that can be estimated experimentally or derived from material properties such as the volume fraction of solids, F accounts for the difference between the thermal conductivities of ice and water in soils (–), C_w is the specific soil moisture capacity (cm^{-1}).

Enhancing an agro-ecosystem model (AHC) for coupled simulation of water-vapor-heat-salt transport in freezing and thawing soils

Appendix B. Supplementary data

Supplementary data to this article can be found online at <https://doi.org/10.1016/j.jhydrol.2025.133640>.

Data availability

Data will be made available on request.

References

- Ahuja, L., Rojas, K.W., Hanson, J.D., 2000. Root Zone Water Quality Model: Modelling Management Effects on Water Quality and Crop Production. Water Resources Publication.
- Allen, R.G., Pereira, L.S., Raes, D., Smith, M., 1998. Crop evapotranspiration: guidelines for computing crop water requirements. In: FAO Irrigation and Drainage Paper No. 56. FAO, Rome, Italy.
- Bloomsburg, G.L., Wang, S.J., 1969. Effect of Moisture Content on Permeability of Frozen Soils. University of Idaho.
- Campbell, G.S., 1985. Soil Physics with BASIC: Transport Models for Soil-plant Systems. Elsevier.
- Cary, J.W., Mayland, H.F., 1972. Salt and water movement in unsaturated frozen soil. Soil Sci. Soc. Am. J. 36, 549–555. <https://doi.org/10.2136/sssaj1972.0361595003600040019x>.
- Dawes, W.R., 1993. Efficient Numerical Solution of Differential Equations for Coupled Water and Solute Dynamics. CSIRO, Institute of Natural Resources and Environment, Division of Water Resources.
- De Vries, D.A., 1963. Thermal properties of soils. Physics of plant environment, 210–235. <https://doi.org/10.1016/B978-0-12-244350-3.3.00006-9>.
- Dorigo, W.A., Zurita-Milla, R., de Wit, A.J., Brazile, J., Singh, R., Schaepman, M.E., 2007. A review on reflective remote sensing and data assimilation techniques for enhanced agroecosystem modeling. Int. J. Appl. Earth Obs. Geoinf. 9, 165–193. <https://doi.org/10.1016/j.jag.2006.05.003>.
- Feddes, R.A., Kabat, P., Van Balkel, P., Bronswijk, J., Halbertsma, J., 1988. Modelling soil water dynamics in the unsaturated zone—state of the art. J. Hydrol. 100, 69–111. [https://doi.org/10.1016/0022-1694\(88\)90182-5](https://doi.org/10.1016/0022-1694(88)90182-5).
- Fernández, A., 1998. An energy balance model of seasonal snow evolution. Phys. Chem. Earth 23, 661–666. [https://doi.org/10.1016/S0079-1946\(98\)00107-4](https://doi.org/10.1016/S0079-1946(98)00107-4).
- Flerchinger, G.N., 2024. The simultaneous heat and water (SHAW) model: User’s manual, Version 3.03-CO₂, with provisions for CO₂ fluxes. Northwest Watershed Research Center USDA Agricultural Research Service, Boise, Idaho. Technical report NWRC 2024-02.
- Flerchinger, G.N., 2000. The Simultaneous Heat and Water (SHAW) Model: Technical Documentation. Northwest Watershed Research Center USDA Agricultural Research Service, Boise, Idaho.
- Flerchinger, G.N., Saxton, K.E., 1989. Simultaneous heat and water model of a freezing snow-residue-soil system i. Theory and development. Trans. Asae 32, 565–571. <https://doi.org/10.13031/2013.31040>.
- Fuchs, M., Campbell, G.S., Papendick, R.I., 1978. An analysis of sensible and latent heat flow in a partially frozen unsaturated soil. Soil Sci. Soc. Am. J. 42, 379–385. <https://doi.org/10.2136/sssaj1978.03615995004200030001x>.
- Hansen, S., 2002. Daisy, a flexible soil-plant-atmosphere system model. Report. Dept. Agric.
- Hansson, K., Šimůnek, J., Mizoguchi, M., Lundin, L., Van Genuchten, M.T., 2004. Water flow and heat transport in frozen soil: numerical solution and freeze-thaw applications. Vadose Zone J. 3, 693–704. <https://doi.org/10.2113/3.2.693>.
- He, H., Liu, L., 2024. Study on irrigation scheme and nitrogen application to sunflower (*Helianthus annuus* L.) in saline farmland in the arid/semi-arid region of hetao irrigation district. Irrig. Sci. 1–17. <https://doi.org/10.1007/s00271-024-00928-4>.
- Heinen, M., Mulder, M., van Dam, J., Bartholomeus, R., van Lier, Q.D.J., de Wit, J., de Wit, A., Hack-Ten Broeke, M., 2024. SWAP 50 years: advances in modelling soil-water-atmosphere-plant interactions. Agric. Water Manag. 298, 108883. <https://doi.org/10.1016/j.agwat.2024.108883>.
- Hillel, D., 1998. Environmental Soil Physics: Fundamentals, Applications, and Environmental Considerations. Academic Press.
- Holzworth, D.P., Huth, N.J., Devol, P.G., et al., 2014. APSIM—evolution towards a new generation of agricultural systems simulation. Environ. Modell. Softw. 62, 327–350. <https://doi.org/10.1016/j.envsoft.2014.07.009>.
- Hu, G., Zhao, L., Li, R., Park, H., Wu, X., Su, Y., Guggenberger, G., Wu, T., Zou, D., Zhu, X., Zhang, W., Wu, Y., Hao, J., 2023. Water and heat coupling processes and its simulation in frozen soils: current status and future research directions. Catena 222, 106844. <https://doi.org/10.1016/j.catena.2022.106844>.
- Huang, Z., Zhang, J., Ren, D., Hu, J., Xia, G., Pan, B., 2022. Modeling and assessing water and nitrogen use and crop growth of peanut in semi-arid areas of Northeast China. Agric. Water Manag. 267, 107621. <https://doi.org/10.1016/j.agwat.2022.107621>.
- Ireson, A.M., Van Der Kamp, G., Ferguson, G., Nachshon, U., Wheater, H.S., 2013. Hydrogeological processes in seasonally frozen northern latitudes: understanding, gaps and challenges. Hydrogeol. J. 21, 53. <https://doi.org/10.1007/s10040-012-0916-5>.
- Kelleners, T.J., 2013. Coupled water flow and heat transport in seasonally frozen soils with snow accumulation. Vadose Zone J. 12, 1–11. <https://doi.org/10.2136/vzj2012.0162>.
- Kimball, B.A., Thorp, K.R., Boote, K.J., et al., 2023. Simulation of evapotranspiration and yield of maize: an inter-comparison among 41 maize models. Agric. For. Meteorol. 333, 109396. <https://doi.org/10.1016/j.agrformet.2023.109396>.
- Kirkham, D., Powers, W.L., 1972. Advanced Soil Physics. Wiley-Interscience.
- Kroes, J.G., van Dam, J.C., Bartholomeus R.P., Gronendijk P., Heinen M., Hendriks R.F. A., Mulder H.M., Supit I., van Walsum P.E.V., 2017. SWAP version 4: Theory description and user manual. Wageningen, Wageningen Environmental Research, Report 2780. <https://doi.org/10.18174/416321>.
- Kroes, J.G., van Dam, J.C., 2003. Reference Manual SWAP version 3.0.3, Alterra-report 773. Green World Research, Wageningen.
- Kurylyk, B.L., Watanabe, K., 2013. The mathematical representation of freezing and thawing processes in variably-saturated, non-deformable soils. Adv. Water Resour. 60, 160–177. <https://doi.org/10.1016/j.advwatres.2013.07.016>.
- Kustas, W.P., Rango, A., Uijlenhoet, R., 1994. A simple energy budget algorithm for the snowmelt runoff model. Water Resour. Res. 30, 1515–1527. <https://doi.org/10.1029/94WR00152>.
- Li, Q., Sun, S., Xue, Y., 2010. Analyses and development of a hierarchy of frozen soil models for cold region study. J. Geophys. Res.: Atmos. 115. <https://doi.org/10.1029/2009JD012530>.
- Li, Y., Xu, X., Chen, Z., Xiong, Y., Huang, Q., Huang, G., 2023. A process simulation-based framework for resource, food, and ecology trade-off by optimizing irrigation and N management. J. Hydrol. 617, 129035. <https://doi.org/10.1016/j.jhydrol.2022.129035>.
- Li, Y., Zhou, J., Kinzelbach, W., Cheng, G., Li, X., Zhao, W., 2013. Coupling a SVAT heat and water flow model, a stomatal-photosynthesis model and a crop growth model to simulate energy, water and carbon fluxes in an irrigated maize ecosystem. Agric. For. Meteorol. 176, 10–24. <https://doi.org/10.1016/j.agrformet.2013.03.004>.

- Li, Z., Ma, L., Flerchinger, G.N., Ahuja, L.R., Wang, H., Li, Z., 2012. Simulation of overwinter soil water and soil temperature with SHAW and RZ-SHAW. *Soil Sci. Soc. Am. J.* 76, 1548–1563. <https://doi.org/10.2136/sssaj2011.0434>.
- Liu, S., Zhang, W., Huang, Q., Wang, R., Huang, G., 2024. Assessment of irrigation and groundwater management strategies in cold arid areas with shallow groundwater tables using a coupled year-round agro-hydrological model. *J. Hydrol.* 632, 130858. <https://doi.org/10.1016/j.jhydrol.2024.130858>.
- Luo, W., Skaggs, R.W., Chescheir, G.M., 2000. DRAINMOD modifications for cold conditions. *Trans. ASAE* 43, 1569–1582. <https://doi.org/10.13031/2013.3057>.
- Mao, W., Zhu, Y., Wu, J., Ye, M., Yang, J., 2020. Modelling the salt accumulation and leaching processes in arid agricultural areas with a new mass balance model. *J. Hydrol.* 591, 125329. <https://doi.org/10.1016/j.jhydrol.2020.125329>.
- Mizoguchi, M., 1990. Water, Heat and Salt Transport in Freezing Soil. University of Tokyo.
- Mu, D., Xun, Y., Gao, Y., Ren, D., Sun, C., Ma, X., Huang, G., Xu, X., 2023. A modified SWAT model for mechanistic simulation of soil water-salt transport and the interactions with shallow groundwater. *Hydrol. Process.* 37, e14980. <https://doi.org/10.1002/hyp.14980>.
- Mualem, Y., 1976. A new model for predicting the hydraulic conductivity of unsaturated porous media. *Water Resour. Res.* 12, 513–522. <https://doi.org/10.1029/WR012i003p00513>.
- Painter, S.L., 2011. Three-phase numerical model of water migration in partially frozen geological media: model formulation, validation, and applications. *Comput. Geosci.* 15, 69–85. <https://doi.org/10.1007/s10596-010-9197-z>.
- Pferdmenges, J., Breuer, L., Jullich, S., Kraft, P., 2020. Review of soil phosphorus routines in ecosystem models. *Environ. Model. Softw.* 126, 104639. <https://doi.org/10.1016/j.envsoft.2020.104639>.
- Ramos, T.B., Darouich, H., Oliveira, A.R., Farzamian, M., Monteiro, T., Castanheira, N., Paz, A., Alexandre, C., Gonçalves, M.C., Pereira, L.S., 2023. Water use, soil water balance and soil salinization risks of Mediterranean tree orchards in southern Portugal under current climate variability: Issues for salinity control and irrigation management. *Agric. Water Manag.* 283, 108319. <https://doi.org/10.1016/j.agwat.2023.108319>.
- Ren, D., Xu, X., Hao, Y., Huang, G., 2016. Modeling and assessing field irrigation water use in a canal system of Hetao, upper Yellow River basin: application to maize, sunflower and watermelon. *J. Hydrol.* 532, 122–139. <https://doi.org/10.1016/j.jhydrol.2015.11.040>.
- Šimůnek, J., Brunetti, G., Jacques, D., van Genuchten, M.T., Aejna, M., 2024. Developments and applications of the HYDRUS computer software packages since 2016. *Vadose Zone J.*, e20310. <https://doi.org/10.1002/vzj2.20310>.
- Šimůnek, J., Van Genuchten, M.T., Aejna, M., 2016. Recent developments and applications of the HYDRUS computer software packages. *Vadose Zone J.* 15. <https://doi.org/10.2136/vzj2016.04.0033>.
- Šimůnek, J., Van Genuchten, M.T., Sejna, M., 2005. The HYDRUS-1D software package for simulating the one-dimensional movement of water, heat, and multiple solutes in variably-saturated media. *University of California-Riverside Research Reports* 1–240.
- Sinclair, T.R., Seligman, N.A., 2000. Criteria for publishing papers on crop modeling. *Field Crops Res.* 68, 165–172. [https://doi.org/10.1016/S0378-4290\(00\)00105-2](https://doi.org/10.1016/S0378-4290(00)00105-2).
- Singh, R., Kroes, J.G., Van Dam, J.C., Feddes, R.A., 2006. Distributed ecohydrological modelling to evaluate the performance of irrigation system in sirsa district, india: i. Current water management and its productivity. *J. Hydrol.* 329, 692–713. <https://doi.org/10.1016/j.jhydrol.2006.03.037>.
- Soldevilla-Martinez, M., Quemada, M., López-Urrea, R., Muñoz-Carpena, R., Lizaso, J.I., 2014. Soil water balance: comparing two simulation models of different levels of complexity with lysimeter observations. *Agric. Water Manag.* 139, 53–63. <https://doi.org/10.1016/j.agwat.2014.03.011>.
- Tang, X., Liu, H., Zhang, Z., Zheng, C., She, Y., Lu, W., 2024. Adaptation of sprinkler irrigation scheduling and winter wheat variety to cope with climate change in the North China plain. *Agric. Water Manag.* 301, 108929. <https://doi.org/10.1016/j.agwat.2024.108929>.
- Tarnawski, V.R., Wagner, B., 1992. A new computerized approach to estimating the thermal properties of unfrozen soils. *Can. Geotech. J.* 29, 714–720. <https://doi.org/10.1139/t92-079>.
- Van Dam, J.C., Huygen, J., Wesseling, J.G., Feddes, R.A., Kabat, P., Van Walsum, P., Groenendijk, P., Van Diepen, C.A., 1997. Theory of SWAP version 2.0; Simulation of water flow, solute transport and plant growth in the soil-water-atmosphere-plant environment, in: DLO Winand Staring Centre.
- van Genuchten, M.T., 1980. A closed-form equation for predicting the hydraulic conductivity of unsaturated soils. *Soil Sci. Soc. Am. J.* 44, 892–898. <https://doi.org/10.2136/sssaj1980.03615995004400050002x>.
- Vanclooster, M., Viaene, P., Diels, J., Feyen, J., 1995. A deterministic evaluation analysis applied to an integrated soil-crop model. *Ecol. Model.* 81, 183–195. [https://doi.org/10.1016/0304-3800\(94\)00170-M](https://doi.org/10.1016/0304-3800(94)00170-M).
- Wan, H., Bian, J., Zhang, H., Li, Y., 2021. Assessment of future climate change impacts on water-heat-salt migration in unsaturated frozen soil using CoupModel. *Front. Environ. Sci.* 15, 10. <https://doi.org/10.1007/s11783-020-1302-5>.
- Wu, M., Wu, J., Tan, X., Huang, J., Jansson, P., Zhang, W., 2019. Simulation of dynamical interactions between soil freezing/thawing and salinization for improving water management in cold/arid agricultural region. *Geoderma* 338, 325–342. <https://doi.org/10.1016/j.geoderma.2018.12.022>.
- Wu, T., Li, H., Hang, L., 2023. Effect of freeze-thaw process on heat transfer and water migration between soil water and groundwater. *J. Hydrol.* 617, 128987. <https://doi.org/10.1016/j.jhydrol.2022.128987>.
- Xie, H., Jiang, X., Tan, S., Wan, L., Wang, X., Liang, S., Zeng, Y., 2021. Interaction of soil water and groundwater during the freezing-thawing cycle: field observations and numerical modeling. *Hydrol. Earth Syst. Sci.* 25, 4243–4257. <https://doi.org/10.5194/hess-25-4243-2021>.
- Xiong, L., Xu, X., Ren, D., Huang, Q., Huang, G., 2019. Enhancing the capability of hydrological models to simulate the regional agro-hydrological processes in watersheds with shallow groundwater: based on the SWAT framework. *J. Hydrol.* 572, 1–16. <https://doi.org/10.1016/j.jhydrol.2019.02.043>.
- Xu, X., Huang, G., Qu, Z., Pereira, L.S., 2010. Assessing the groundwater dynamics and impacts of water saving in the Hetao irrigation district, Yellow River Basin. *Agric. Water Manag.* 98, 301–313. <https://doi.org/10.1016/j.agwat.2010.08.025>.
- Xu, X., Huang, G., Sun, C., Pereira, L.S., Ramos, T.B., Huang, Q., Hao, Y., 2013. Assessing the effects of water table depth on water use, soil salinity and wheat yield: searching for a target depth for irrigated areas in the upper Yellow River basin. *Agric. Water Manag.* 125, 46–60. <https://doi.org/10.1016/j.agwat.2013.04.004>.
- Xu, X., Sun, C., Huang, G., Mohanty, B.P., 2016. Global sensitivity analysis and calibration of parameters for a physically-based agro-hydrological model. *Environ. Model. Softw.* 83, 88–102. <https://doi.org/10.1016/j.envsoft.2016.05.013>.
- Xu, X., Sun, C., Huang, G.H., 2023. The agro-hydrological & chemical and crop systems simulator (AHC)-theoretical documentation (version 2.01), in: China Agricultural University (Beijing). Research report for version 2.01 (166 pages).
- Xu, X., Sun, C., Neng, F., Fu, J., Huang, G., 2018. AHC: an integrated numerical model for simulating agroecosystem processes—model description and application. *Ecol. Model.* 390, 23–39. <https://doi.org/10.1016/j.ecolmodel.2018.10.015>.
- Xun, Y., Xiao, X., Sun, C., Meng, H., Gao, Y., Huang, G., Xu, X., 2022. Modeling heat-water-salt transport, crop growth and water use in arid seasonally frozen regions with an improved coupled SPAC model. *J. Hydrol.* 615, 128703. <https://doi.org/10.1016/j.jhydrol.2022.128703>.
- Zheng, C., Šimůnek, J., Zhao, Y., Lu, Y., Liu, X., Shi, C., Li, H., Yu, L., Zeng, Y., Su, Z., 2021. Development of the Hydrus-1D freezing module and its application in simulating the coupled movement of water, vapor, and heat. *J. Hydrol.* 598, 126250. <https://doi.org/10.1016/j.jhydrol.2021.1262>.